Ultrasonics Sonochemistry 94 (2023) 106344

Contents lists available at ScienceDirect

Ultrasonics Sonochemistry

journal homepage: www.elsevier.com/locate/ultson

Sustainable extraction of ligustilide and ferulic acid from Angelicae Sinensis Radix, for antioxidant and anti-inflammatory activities

Xuejiao Song, Chang Liu, Yang Zhang, Xiaoyue Xiao, Guorui Han, Kedi Sun, Shuoqi Liu, Zhiyun Zhang, Chunliu Dong, Yadan Zheng, Xueying Chen, Tong Xu, Yanyan Liu *, Yanhua Li *

College of Veterinary Medicine, Northeast Agricultural University, Harbin, Heilongjiang 150030, China

ARTICLE INFO

Keywords:
Energy efficiency
Process innovation
Enzyme and ultrasonic co-assisted aqueous two-phase extraction
Central composite design
Comprehensive evaluation value
Angelicae Sinensis Radix

ABSTRACT

The 2030 Agenda for Sustainable Development envisions a rational use of energy and resources in all technological processes. However, in the extraction methods of compounds from medicinal plants and herbs, there is an urgent to reduce the use of organic solvents and increase the energy efficiency of these methods. Therefore, a sustainable extraction method (enzyme and ultrasonic co-assisted aqueous two-phase extraction, EUA-ATPE) of simultaneous extraction and separation of ferulic acid and ligustilide from Angelicae Sinensis Radix (ASR) was developed by integrating enzyme-assisted extraction (EAE) with ultrasonic-assisted aqueous two-phase extraction (UAE- ATPE). The effects of different enzymes, extraction temperature, pH, ultrasonic time, liquid-to-materials ratio, etc., were optimized by single-factor experiments and central composite design (CCD). Under the optimum conditions, the highest comprehensive evaluation value (CEV) and extraction yield were obtained by EUA-ATPE. Furthermore, recovery (R), partition coefficient (K), and scanning electron microscopy (SEM) analysis revealed that enzyme and ultrasonic treatment improved mass transfer diffusion and increased the degree of cell disruption. Besides, the EUA-ATPE extracts have shown great antioxidant and anti-inflammatory activity in vitro. Finally, compared to different extraction methods, EUA-ATPE achieved higher extraction efficiency and higher energy efficiency due to the synergistic effect between EAE and UAE-ATPE. Therefore, the EUA-ATPE provides a sustainable method for extracting bioactive compounds from medicinal plants and herbs, contributing to Sustainable Development Goals (SDG), including SDG-6, SDG-7, SDG-9, SDG-12, and SDG-15.

1. Introduction

Nowadays, although the world is making rapid progress towards development and prosperity, it still faces new and more difficult challenges at all levels. The challenges that are becoming more and more striking in our everyday life include environmental protection and issues regarding climate change and so on. As a response to all the new challenges of modern society, the United Nations launched the 2030 Agenda for Sustainable Development. The 2030 Agenda includes the 17 Sustainable Development Goals (SDGs) and 169 associated targets [1]. For a long time, the process of plant extraction may produce waste liquid and waste material that pollute the environment, and the extraction process may not be optimized enough to efficiently use of the active ingredients of drugs. This experiment innovates the extraction process of Angelicae Sinensis Radix (ASR) and provides new ideas for the extraction of other plants in the future.

ASR is a valuable resource of traditional Chinese medicine (TCM) that comes from the root of an umbrella plant *Angelica sinensis* (Oliv.) Diels [2]. ASR has been widely used in the treatment of gynecological diseases such as dysmenorrhea, cardiovascular diseases and cerebrovascular diseases for centuries in TCM [3]. Accordingly, modern pharmacological studies gradually had realized ASR anti-inflammatory effect [4] such as therapeutic effect for hepatitis [5] and inflammation induced by subcutaneous, carrageenan or lipopolysaccharides (LPS) [6,7]. ASR contains a variety of plant active components, mainly including polysaccharides, ferulic acid (FA), amino acids and ligustilide (LIG) and so on [8]. FA (4-hydroxyl-3-methoxy-cinnamic acid) is a kind of phenolic acid, and it has the potential to be utilized in the field of food, pharmaceutical and biomedical industries due to its diverse physiological functions, such as antioxidant, antimicrobial and anti-inflammatory properties. Besides, LIG also has anti-inflammatory activities such as alleviating colitis effect by inhibiting the NF-κB, AP-1 and MAPK

* Corresponding authors at: College of Veterinary Medicine, Northeast Agricultural University, 600 Changjiang Road, Xiangfang, Harbin, Heilongjiang 150030, China.

E-mail addresses: Liuyanyan@neau.edu.cn (Y. Liu), Liyanhua@neau.edu.cn (Y. Li).

https://doi.org/10.1016/j.ultsonch.2023.106344
Received 18 November 2022; Received in revised form 6 February 2023; Accepted 21 February 2023
Available online 24 February 2023

Table 1
Example of some research that advances the SDGs.

The focus of the study	Key points	SDGs and targets	Countries of affiliation (authors)	Reference
Enhance co-production of glabridin and isoliquiritigenin	• Ultrasound-assisted deep eutectic solvents enhanced glabridin and isoliquiritigenin productoin. • Glabridin and isoliquiritigenin have antioxidant activities, anti-inflammatory activities, and antibacterial activities.	SDG-6: Ensure availability and sustainable management of water and sanitation for all. Target 6.3 SDG-3: Ensure healthy lives and promote well-being for all at all ages Target 3.9	China	[15]
Enhance production of resveratrol from P. cuspidatum	• Enzyme-assisted ultrasonic approach for highly efficient extraction of resveratrol from P. cuspidatum.	SDG-3: Ensure healthy lives and promote well-being for all at all ages. Target 3.9	China	[82]
Enhance co-production of essential oil and flavonoids from Baeckea frutescens	• Enzyme pretreatment combined with ultrasonic-microwave-assisted surfactant for simultaneous extraction of essential oil and flavonoids. • Antibacterial activities.	SDG-3: Ensure healthy lives and promote well-being for all at all ages. Target 3.9	China	[20]
Enhance production of Polysaccharides from Malus hupehensis	• Ultrasonic-Assisted Aqueous Two-Phase Extraction and Properties of Water-Soluble Polysaccharides. • Polysaccharides showed a significant antioxidant capacity, and an inhibition activity of α-glucosidase.	SDG-7: Ensure access to affordable, reliable, sustainable and modern energy for all. Target 7.a SDG-3: Ensure healthy lives and promote well-being for all at all ages. Target 3.9	China	[22]
Enhance yield and quality of essential oil	• Ultrasonic-microwave assisted method preceded by enzymolysis treatment to extract essential oil. • Essential oil as food additives in food industries to prevent the oxidation and bacterial spoilage.	SDG-12: Ensure sustainable consumption and production patterns. Target 12.2 SDG-3: Ensure healthy lives and promote well-being for all at all ages. Target 3.4	China	[45]
Enhance co-production of protein and antioxidant compounds	• Enzyme and ultrasound assisted extraction to enhance recovery of protein. • High phenolic compound to improve antioxidant capacity values.	SDG-6: Ensure availability and sustainable management of water and sanitation for all. Target 6.3 SDG-3: Ensure healthy lives and promote well-being for all at all ages. Target 3.9	Turkey	[83]

pathways [9,10]. However, the practical applications of FA and LIG are limited due to their physico-chemical properties of poor water solubility, thermolability and weak photostability [11,12]. Simultaneously, traditional extraction methods have many shortages such as prolonged heating induced the degradation of compounds, poor extraction efficiency or the need for numerous amounts solvent that is inconsistent with SDGs. Hence, it is pivotal to use a more environmentally friendly extraction method to extract FA and LIG at the same time.

Currently, the extraction industry is moving fast into sustainable processes based on the implementation of ecologically friendly extraction methods in the food and pharmaceutical industries. For the purpose of sustainable development, a number of novel techniques such as aqueous two phase extraction (ATPE), enzyme-assisted extraction (EAE) [13], ultrasonic-assisted extraction (UAE) [14], and deep eutectic solvents-assisted extraction (DESE) [15,16]have been developed because of in line with sustainable development strategies [17]. For example, water-phase enzyme extraction has become a green phytochemical extraction technology [18]. Enzyme assisted extraction can be used to enhance the release of secondary metabolites from plant matrix. It possesses the advantages of compatibility with the environment, ease of operating and high efficiency [19,20]. Similarly, ultrasound assisted extraction is also regarded as an environmentally friendly extraction method due to its low energy and solvent consumption, improved extraction yield, and short extraction time. In addition, ultrasound can produce cavitation bubbles that upon bursting, and then cavitation bubbles releasing energy in the form of heat which enhance mass transfer and finally reduce organic solvent consumption [21]. Nowadays, ATPE has gradually spread from separation to extraction and purification due to its high yield and relatively environment-friendly features than pure organic solvents [22]. The separation and purification capability of ATPE was focused on the biphasic extraction capacity and selectivity, and thus the success of ATPE was largely dependent on the composition of aqueous two-phase system (ATPS) which usually consists of a polymer and a salt, or short-chain ethanol and a salt. In this way, the target compound was selectively transferred to one phase, whereas co-existed impurities can be extracted to the other phase. The following Table 1 includes recent research on extraction in SDGs, and these studies have used ultrasound or ultrasound combined with other technologies.

Since each green extraction method has unique advantages, the combined novel technologies has been accepted widespread concern for its higher extraction rates. For example, enzyme-assisted aqueous two-phase extraction (EA-ATPE) method and EAE combined with microwave-assisted aqueous two-phase extraction (MAATPE) method were used to extraction recently [23,24]. In order to preliminarily release, extract and purify the active components in ASR, this study combined EAE with UA-ATPE innovatively. This experiment combined the structural characteristics of ASR and characteristics of active ingredients that contain a large amount of fiber with FA and LIG's physicochemical properties of unstable as well as poor solubility. To improve the extraction efficiency, reduce the extraction time, and reduce the obstruction of cellulose, therefore, combining with literature researching, it is suggested that the combination of EAE and UA-ATPE may improve the extraction efficiency and reduce the use of organic solvents to achieve sustainable development.

To maximize resource efficiency, optimal extraction parameters in EUA-ATPE were investigated by single factor experiments and central composite design (CCD) to obtain maximize the comprehensive evaluation value (CEV). Response surface methodology (RSM) with statistical experimental designs are typically employed in the optimization of novel extraction procedures [25]. RSM functions as a visual service to display the clear image of the effects concerning several extraction parameters and also guide to trace the sections where extraction can be optimized [26]. CCD is a kind of RSM to determine the fitting between polynomial equation and experimental graph and had achieved outstanding result [27]. FA and LIG obtained from the top phases were detected by high performance liquid chromatography (HPLC) and then scanning electron microscopy (SEM) were used to observed surface morphology of the samples for exploring the extraction mechanism in EUA-ATPE process. Considering the FA belonging phenolic acid, ASR extracts by EUA-ATPE were investigated by antioxidant activity assays of scavenging ABTS and ferric ion reducing antioxidant power (FRAP) assay. Finally, anti-inflammatory activity was assessed by measuring the NO, iROS, PGE_2, IL-6, IL-1β, TNF-α and relevant mRNA expression in LPS-induced RAW264.7 cells. These anti-inflammatory and antioxidant abilities is conducive to human psychological and physical health,

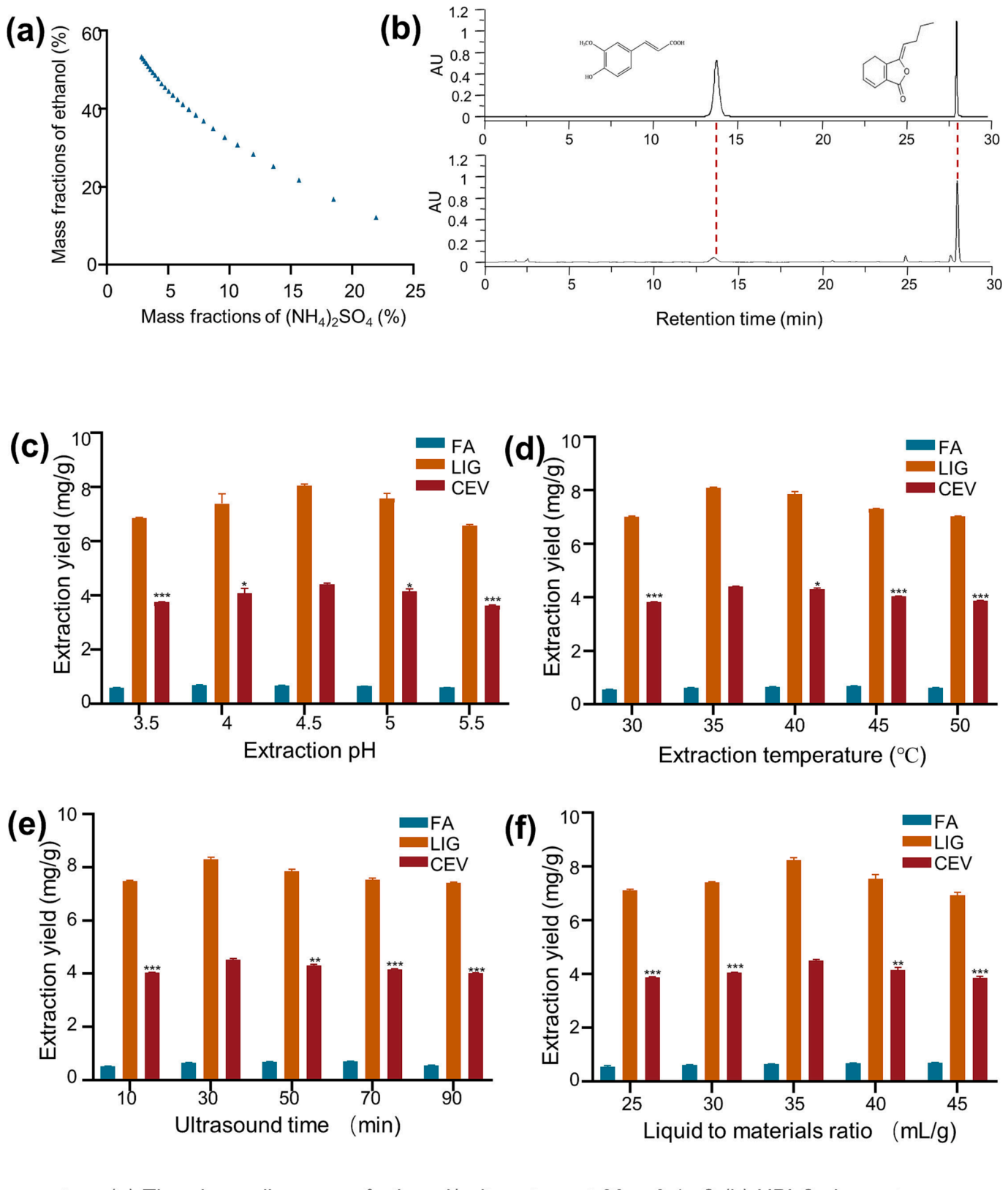

Fig. 1. (a) The phase diagrams of ethanol/salt system at 20 ± 0.1 ℃. (b) HPLC chromatograms of standards (FA and LIG) and extracts by EUA-ATPE. The effects of different Extraction pH (c), Extraction temperature (d), Ultrasound time (e) and Liquid-to-material ratio (f) on extraction yields and CEV. *** Most significant ($p < 0.001$). ** More significant ($p < 0.01$). * Significant ($p < 0.05$).

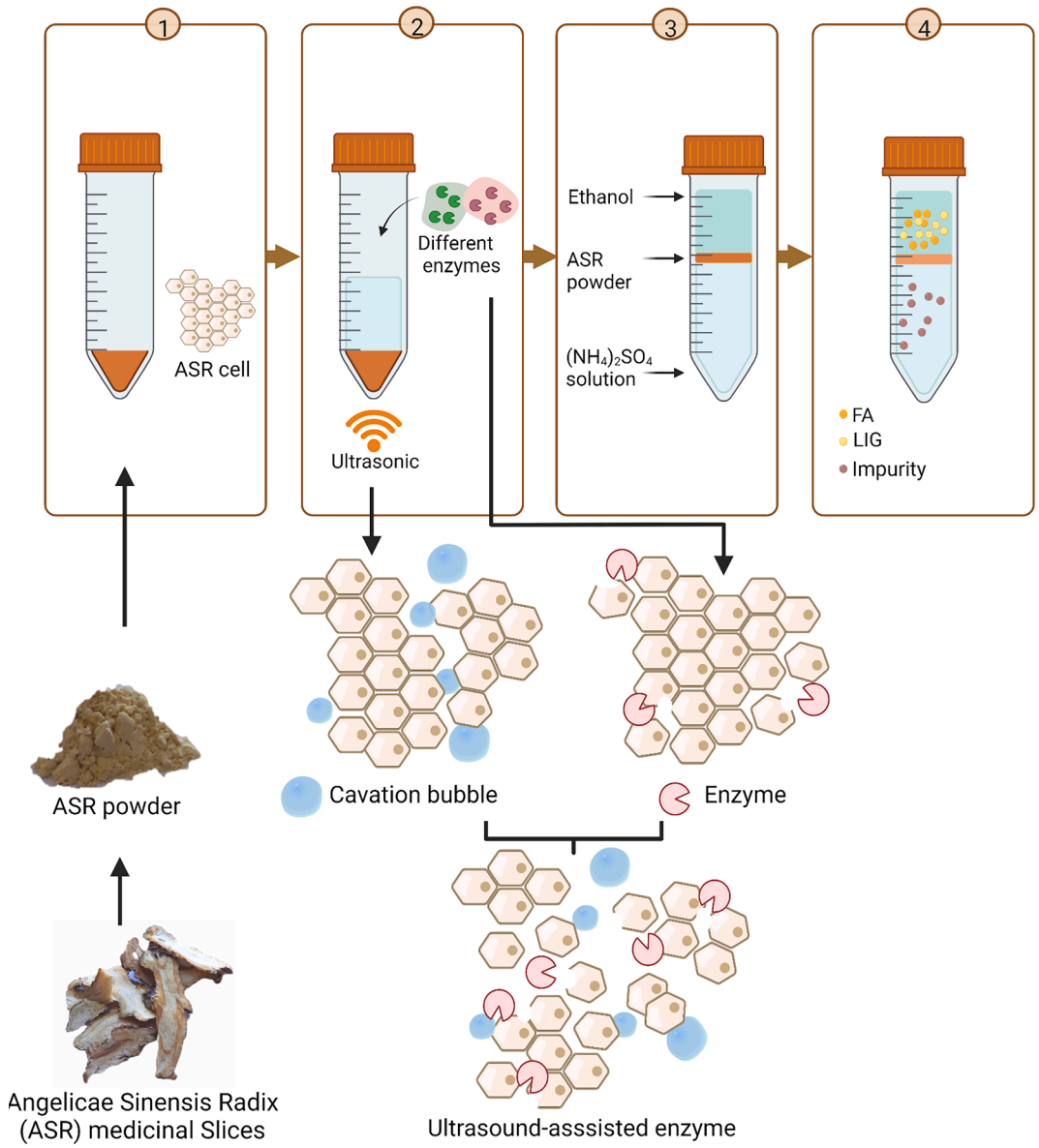

Fig. 2. The schematic of the apparatus of EUA-ATPE.

which is consistent with SDGs 3.

2. Materials and methods

2.1. Materials and reagents

Decoction pieces of ASR were purchased from Shijiazhuang Yiling Traditional Chinese Medicine Slices Co., Ltd. (Shijiazhuang, China). Subsequently, authenticated by associate professor Yu Dan (Department of Chinese Medicine, Heilongjiang University, Harbin, China), and these decoction pieces were grounded into powders (150 mesh). Then, powder was stored in a sealed bag at 4 °C. Papain, neutral protease and xylanase were obtained from Maclean Biochemical Co., Ltd. (Shanghai, China). Cellulase, hemicellulase, pectinase and lipopolysaccharides (LPS) were purchased from Beijing Solarbio Science & Technology Co., Ltd. (Beijing, China). Ligustilide standard and ferulic acid standard were obtained from Chengdu Herbpurify CO., LTD (Chengdu, China). Chromatographic-grade acetonitrile were purchased from Dikma Technologies Inc. (Beijing, China). Ethanol, hydrochloric acid, citric acid, $(NH_4)_2SO_4$ and Na_2HPO_4 were obtained from Kermel Chemical Reagents Co., LTD (Tianjin, China). Other reagents were all of analytical grade or better.

2.2. Phase diagram and single factor optimization

2.2.1. Plotting phase diagram of ATPS

Anhydrous ethanol, salt and distilled water were employed to form ATPS in this work. When the mass fractions of salts were maintained at a high level, the curve would result in the extreme points of forming ATPS with the continuous increase of ethanol concentration. Therefore, the mass fractions of ethanol and phase-forming salts should be firstly chosen from regions above binodal curve prior to the following experiments [28]. The phase diagram was prepared by turbidity titration method at 20 ± 0.1 °C based on the method previously described by Cheng Z, et al [29] and made some modification. At first, certain amounts of $(NH_4)_2SO_4$ solution with known mass fraction were put into a 100 mL conical flask. Then, anhydrous ethanol was added into the mixture dropwise, followed by the fully blending with heating magnetic stirring apparatus. Initially, it can be observed that the solution was pellucid, but after a certain amount of absolute ethanol was added, one

Table 2
CCD experiments design (four independent variables and their coded levels) and results.

Variables	Name	Coded Levels				
		−2	−1	0	1	2
X_1	pH	3	3.5	4	4.5	5
X_2	Temperature (℃)	25	30	35	40	45
X_3	Liquid to materials ratio (mL/g)	25	30	35	40	45
X_4	Ultrasound time (min)	0	10	30	50	70

Run	X_1	X_2	X_3	X_4	FA (mg/g)	LIG (mg/g)	CEV
1	3.5 (-1)	30 (-1)	30 (-1)	10 (-1)	0.59	8.9	4.39
2	4.5 (1)	30 (-1)	30 (-1)	10 (-1)	0.64	7.68	4.8
3	3.5 (-1)	40(1)	30 (-1)	10 (-1)	0.77	8.17	4.25
4	4.5 (1)	40(1)	30 (-1)	10 (-1)	0.67	7.18	4.51
5	3.5 (-1)	30 (-1)	40(1)	10 (-1)	0.67	8.03	4.15
6	4.5 (1)	30 (-1)	40(1)	10 (-1)	0.69	7.82	4.59
7	3.5 (-1)	40(1)	40(1)	10 (-1)	0.69	7.77	3.96
8	4.5 (1)	40(1)	40(1)	10 (-1)	0.72	7.27	4.16
9	3.5 (-1)	30 (-1)	30 (-1)	50(1)	0.64	7.58	4.26
10	4.5 (1)	30 (-1)	30 (-1)	50(1)	0.61	7.89	4.3
11	3.5 (-1)	40(1)	30 (-1)	50(1)	0.74	7.49	4.16
12	4.5 (1)	40(1)	30 (-1)	50(1)	0.74	7.67	4.13
13	3.5 (-1)	30 (-1)	40(1)	50(1)	0.69	7.92	4.2
14	4.5 (1)	30 (-1)	40(1)	50(1)	0.68	8.4	4.35
15	3.5 (-1)	40(1)	40(1)	50(1)	0.67	7.55	4.27
16	4.5 (1)	40(1)	40(1)	50(1)	0.67	7.5	4.04
17	3(-2)	35(0)	35(0)	30(0)	0.61	7.23	4.33
18	5(2)	35(0)	35(0)	30(0)	0.73	7.53	4.7
19	4(0)	25 (-2)	35(0)	30(0)	0.72	7.67	4.24
20	4(0)	45(2)	35(0)	30(0)	0.75	6.8	3.81
21	4(0)	35(0)	25 (-2)	30(0)	0.78	8.66	4.17
22	4(0)	35(0)	45(2)	30(0)	0.73	8.74	3.96
23	4(0)	35(0)	35(0)	0(-2)	0.72	8.35	4.39
24	4(0)	35(0)	35(0)	70(2)	0.73	7.35	4.08
25	4(0)	35(0)	35(0)	30(0)	0.75	8.54	4.77
26	4(0)	35(0)	35(0)	30(0)	0.73	8.8	4.78
27	4(0)	35(0)	35(0)	30(0)	0.72	7.98	4.81
28	4(0)	35(0)	35(0)	30(0)	0.7	8.61	4.58
29	4(0)	35(0)	35(0)	30(0)	0.73	8.76	4.69
30	4(0)	35(0)	35(0)	30(0)	0.67	7.91	4.79

further drop made the solution turbid and separated into two phases spontaneously. Finally, a few drops of distilled water were added to make the mixture clear again, and both mass fractions of ethanol and distilled water were recorded exactly. Above procedures were repeated about sixty times in order to acquire enough data and construct the phase diagrams (Fig. 1 a).

2.2.2. Single factor optimization

Single factor experiments were utilized to optimize the extraction parameters. Firstly, ASR powder and different enzymes were added to the prepared buffer solution with a certain liquid–solid ratio. Enzyme incubations were performed by papain (Pap), neutral protease (Nep), xylanase (Xyl), cellulase (Cel), hemicellulose (Hem), pectinase (Pec) and the combination of both enzymes, and adjust the pH of the enzymatic hydrolysate with NaOH or HCl. Besides, ultrasonic power was optimized from 300 W to 700 W. Furthermore, the concentration ranges of ethanol and $(NH_4)_2SO_4$ were respectively 20–40% (w/w) and 14–22% (w/w) in the ATPS, which were determined according to the phase diagram. Then, total extraction time (total extraction time is equal to ultrasonic time plus water bath time) was optimized from 60 min to 180 min. Finally, follow the step in 2.5 to determine the FA and LIG content. The CEV in the final extract was used as the index to determine optimal extract condition.

2.3. Extraction by EUA-ATPE

2.3.1. EUA-ATPE procedure

A schematic of the apparatus of EA-ATPE is shown in Fig. 2 (Created with BioRender.com). A total of 0.5 g ASR powder, 16.65 g disodium hydrogen phosphate-citric acid buffer solution and 80 U Cel and 140 U Hem were added to a 50 mL EP tube, mixed evenly by a vortex mixer. Then the mixture was placed in ultrasonic bath (Frequency: 40 kHz, Range of operation: 40–100%, Model: SB25-12DTD (720 W), Ningbo Scientz Biotechnology CO., Ltd, Ningbo, China) and the extraction temperature were fixed at 35 °C for 25 min. Subsequently, the mixture was placed in a water bath at 35 °C for 65 min and then incubated at 85 °C for 5 min to inactivate the enzymes. Based on the phase diagram, 6.06 g of $(NH_4)_2SO_4$, 10.10 mL anhydrous ethanol were added into the buffer solution, and mixed well to form a stable ATPS. Then, the solution was left undisturbed at room temperature for 30 min to form ATPS. Finally, the mixture was centrifuged at 8000 rpm for 5 min to facilitate phase separation and the volumes of the upper phases of the system were recorded after phase separation completed; then, the yields of LIG and FA were determined. The yield (Y) of LIG and FA were defined according to eq (1).

$$Y\left(\mathrm{mg}\Big/\mathrm{g}\right) = \frac{C_t\, V_t}{M} \tag{1}$$

where C_t (mg/mL) represent the concentrations of LIG and FA in the top phases, respectively, while V_t (mL) is the separate volumes of the top phases and M is the total mass of ASR powder.

2.3.2. Optimization of the EUA-ATPE by CCD

Based on single-factor experiments, response surface methodology (RSM) with central composite design (CCD) was used to further optimize the independent variables for highest CEV. The optimal conditions used CCD with four variables (see in Table 2 their coded and uncoded values). The matrix is shown in Table 2 with the 30 experiments involving four variables, each at five levels [30]. In each case, the yields of LIG and FA were quantified to calculate CEV as the index.

Experimental data were fitted to a quadratic polynomial model and the model was explained by the following quadratic equation:

$$Y = \beta_0 + \sum_{i=1}^{4}\beta_i X_i + \sum_{i=1}^{4}\beta_{ii}X_i^2 + \sum_{i=1}^{4}\sum_{j=i+1}^{4}\beta_{ij}X_iX_j \tag{2}$$

where X_i, X_j are the input variables, which influence the response function Y; β_0 is the intercept; β_i, β_{ii}, and β_{ij} are the coefficients of the linear, quadratic, and the interaction term, respectively.

2.3.3. Calculation of comprehensive evaluation value (CEV) by entropy weighting method (EWM)

Information entropy is the measurement of the disorder degree of a system, which can measure the amount of useful information with the data provided. When the difference of the value among the evaluating

objects on same indicator is bigger, the entropy is smaller, and the weight of this indicator should be set correspondingly high. Hence, the entropy theory is an objective way for weight determination. Index components were normalized with the content data of each index component from the test (index component = [measured value − minimum value]/[maximum value – minimum value]) [31], and the weight coefficients of each component were calculated with entropy weighting method (EWM) after the influence of scale and magnitude among the indexes were eliminated, so as to obtain the comprehensive evaluation value (CEV).

There were m objects with n indexes to be evaluated in the index system then the matrix was evaluated as follows [32]:

$$X = \{x_{ij}\}_{m\times n}$$

where x_{ij} referred to the value of the recovery of the j-th component in the i-th sample ($i = 1, 2, 3, \ldots, m$, $j = 1, 2, 3, \ldots, n$).

The detailed formulas of EWM were as follows:

(1) Normalization of indicators:

$$r_{ij} = \frac{x_{ij} - \min\limits_i\{x_{ij}\}}{\left(\max\limits_i\{x_{ij}\} - \min\limits_i\{x_{ij}\}\right)}$$

where r_{ij} was the standardized value of the j-th component in the i-th sample ($i = 1, 2, 3, \ldots, m$, $j = 1, 2, 3, \ldots, n$).

(2) Calculation of the proportion of the j-th index (p_{ij}):

$$p_{ij} = \frac{x_{ij}}{\sum_{i=1}^{n} x_{ij}}, i = 1, \cdots, n; j = 1, \cdots, m$$

(3) Calculation of the entropy value of the j-th index (e_j):

$$e_j = -k\sum_{i=1}^{n} p_{ij} ln p_{ij}, k = 1/lnn$$

(4) Calculation of the information entropy redundancy of the j-th index (d_j):

$$d_j = 1 - e$$

(5) Calculation the entropy weight coefficient (w_j) of the j-th index:

$$w_j = d_j / \sum_{j=1}^{m} d_j \tag{3}$$

Then the comprehensive evaluation value (CEV) was calculated by the following formula:

$$CEV = \sum_{i=1}^{m} Y_{ij} w_j \tag{4}$$

2.4. LC-MS/MS analysis

LC-MS/MS analysis were performed using an ExionLC™ AD system (SCIEX) coupled with a QTRAP®6500 + mass spectrometer (SCIEX) in Novogene Co., Ltd. (Beijing, China). ASR extract by EUA-ATPE was injected into a Xselect HSS T3 (2.1 × 150 mm, 2.5 μm) using a 20 min linear gradient at a flow rate of 0.4 mL/min for the positive/negative polarity mode. The eluents were eluent A (0.1% Formic acid–water) and eluent B (0.1% Formic acid-acetonitrile). The solvent gradient was set as follows: 2% B, 2 min; 2–100% B, 15.0 min; 100% B, 17.0 min; 100–2% B, 17.1 min; 2% B, 20 min. QTRAP® 6500 + mass spectrometer was operated in positive polarity mode with Curtain Gas of 35 psi, Collision Gas of Medium, IonSpray Voltage of 5500 V, Temperature of 550 ℃, IonSource Gas of 1: 60, Ion Source Gas of 2: 60. QTRAP® 6500 + mass spectrometer was operated in negative polarity mode with Curtain Gas of 35 psi, Collision Gas of Medium, IonSpray Voltage of −4500 V, Temperature of 550 ℃, Ion Source Gas of 1: 60, Ion Source Gas of 2: 60.

2.5. Determination of LIG and FA by HPLC

A Waters 2640-DAD high-performance liquid chromatograph with a C_{18} reversed-phase column (Dikema, 4.6 × 250 mm, 5 μm) was used in chromatographic analysis. The chromatographic procedure was adopted with the following conditions: flow rate, 1.0 mL/min; column temperature, 25 °C; detection wavelength, 325 nm; injection volume, 10 μL; mobile phase of 0.2% phosphoric acid aqueous solution (A), and of acetonitrile (B), 0–15 min, 82% −80% A, 15–25 min, 80% −10% A, 25–30 min, 10% −82% A, gradient elution. The products were calculated from the peak areas of the corresponded signals in the chromatogram. The applicability of HPLC analysis for the determination of FA and LIG was evaluated in terms of calibration-curve linearity, inter-day and intra-day precision, stability, repeatability and recovery rate (shown in Supplementary data).

2.6. Comparison of different extraction methods

The extraction effect of EUA-ATPE was compared with the EA-ATPE, UA-ATPE, UAE and Soxhlet extraction (SE). All conditions used for extraction by EA-ATPE, UA-ATPE and UAE were corresponding the EUA-ATPE optimal conditions. The conditions for SE processes are as follows: 1 g ASR powders and 35 mL of ethanol were added to the Soxhlet extractor and placed in water bath for 2 h and kept at a constant temperature of 70 °C. Recovery (R) and partition coefficient (K) of FA and LIG were used to measure the extraction ability, and the parameters were set according to Eq (5) and Eq (6) [33,34], as follows:

$$\mathrm{R}(\%) = \frac{\mathrm{C_t V_t}}{\mathrm{C_t V_t + C_b V_b}} \times 100 \tag{5}$$

$$\mathrm{K} = \frac{\mathrm{C_t}}{\mathrm{C_b}} \tag{6}$$

where C_t and C_b represent FA and LIG concentrations in the top and bottom phases, respectively, and V_t and V_b are the volumes of the top and bottom phases, respectively.

2.7. Scanning electron microscopy observation

Scanning electron microscopy (SEM) was used to observe the morphology of ASR powder after different treatments, including ASR before extraction, after SE, UA-ATPE, EA-ATPE, and EUA-ATPE extraction. The powder was dried and then analyzed by scanning electron microscopy at 5000 × magnification.

2.8. Antioxidant capacity

In order to verify the effectiveness of EUA-ATPE and SE extracts, the antioxidant capacity was tested. Ferric ion reducing antioxidant power (FRAP) was used according to the methods in the literature [35]. In this assessment, precisely 180 μL of the FRAP working solution (prepared with reference [36]) was gently mixed with 5 μL of each extract and left for 5 min. The data of the extracts were recorded at 593 nm. A standard curve was plotted with the $FeSO_4$ solution instead of the sample solution for the test. The fitted equation was Y = 0.29679 X + 0.29679 (R^2 = 0.9993), indicating that 0.15–1.5 mmol/L $FeSO_4$ solution showed a good linear correlation with absorbance. The FRAP value was expressed as the concentration of the standard substance $FeSO_4$ solution.

The method was adapted from previous tests and modified for the ABTS free radical scavenging assay [37]. The ABTS radical scavenging capacities of various samples were conducted with a Total Antioxidant Capacity Assay Kit. The ABTS radical cation (ABTS +) was generated by mixing an aqueous solution of ABTS and oxidant. These reagents reacted in a ratio of 1: 1 (v/v) respectively and were kept to react completely in the dark for 12 h, then diluted to an absorbance of 0.70 ± 0.05 at 735 nm with ethanol. 200 μL ABTS working solution and 10 μL diluted

samples were mixed. After 2–6 min in the dark, the absorbance was measured at 735 nm in a microplate reader. Ascorbic acid was used as the positive control in all the above tests, and ABTS radical scavenging rate (%) = $[1 - (A_2 - A_1)]/ A_0 \times 100$. A_2 was the extract solution with the blank solvent, A_1 was the sample solution with the working solution, and A_0 was the blank solvent with the free radical working solution.

2.9. In vitro anti-inflammatory activity

2.9.1. Cell culture and treatment strategy

Murine macrophage RAW264.7 cells were purchased from the American Type Culture Collection (ATCC, Manassas, VA) and maintained in Dulbecco's modified Eagle's medium (DMEM) supplemented with 10% fetal bovine serum at 37 °C in 5% CO_2 humidified air. Cells at passages 10–20 were used for the experiments.

Macrophages were plated at a density of 1×10^4 cells/well in 96-well plates for 12 h and then stimulated with LPS (1 μg/mL) for 24 h. Afterwards, cells incubated for another 24 h with various treating including 11 groups: (1) control group; (2) model group; (3) high dose EUA-treated (H-EUA) group; (4) middle dose EUA-treated (M−EUA) group; (5) low dose EUA-treated (L-EUA) group; (6) high dose SE-treated (H-SE) group; (7) middle dose SE-treated (M−SE) group; (8) low dose SE-treated (L-SE) group; (9) ligustilide treated group; (9) ferulic acid treated group; (10) monomer mixture-treated group; (11) dexamethasone-treated group (DEX). In the EUA-treated group, the cells were received 2.5 mg/mL, 1.25 mg/mL and 0.625 mg/mL EUA-ATPE extracts, respectively. And in the SE-treated group, the cell received 2.5 mg/mL, 1.25 mg/mL and 0.625 mg/mL SE extracts, respectively. In standers group ligustilide (20 μg/mL), ferulic acid (1.6 μg/mL) and monomer mixture (21.6 μg/mL) were given. The dose of monomeric administration was converted according to the content results in 2.5 mg/mL EUA-ATPE extract. In addition, 1 μM dexamethasone (DEX) was administrated as a positive control. After 24 h of incubation, the supernatants were assayed for their NO, ROS, PGE_2, IL-6, IL-1β and TNF-α levels.

2.9.2. Cell viability assay

1×10^4 cells/well RAW264.7 cells with different treatment were cultured in 96-well plates for 24 h. And then CCK-8 (10 μL per well) [38] solution was added to plates for 1 h incubation. The OD value at the wavelength of 450 nm was measured using a microplate reader.

2.9.3. Determination of intracellular reactive oxygen species (iROS)

To evaluate the production of iROS [39], the RAW264.7 cells were seeded onto 96-well plates at a density of 1×10^4 cells/well. After 12 h, the cells were incubated with LPS (1 μg/mL) for 24 h and one set of the cells were left untreated as the control. Then, 11 sets of the LPS-pretreated cells were co-cultured with various conditions. Subsequently, the cells incubated with 2′, 7′-dichlorofluorescein diacetates (DCFH-DA) (10 μM) in fresh medium at 37 °C for 40 min in the dark and then washed with PBS to remove the extracellular DCFH-DA. The emitted fluorescence was measured at an excitation of 485 nm and an emission of 530 nm using a multimode microplate reader.

2.9.4. Determination of NO

The nitrite concentration in the culture medium as an indicator of NO production was measured by the Griess assay. Briefly, the RAW264.7 cells (1×10^4 /well) were incubated in a 96-well plate for 12 h and treatment with 1 μg/mL LPS for 24 h before pretreated with various conditions for 24 h. After co-cultured for 24 h in a 5% CO_2 incubator at 37 °C, 50 μL of cell culture medium was collected and mixed with 50 μL of Griess reagent I and II, and the mixture was incubated at room temperature for 10 min with horizontal shaking. The OD value of the solution was measured at 540 nm using a microplate reader and the nitrite concentration was then calculated by using sodium nitrite ($NaNO_2$) as a standard.

2.9.5. Determinations of PGE_2 and inflammatory cytokines

The levels of PGE_2 and the pro-inflammatory cytokines TNF-α, IL-1β and IL-6 in cell culture medium were measured by using commercial mouse immunoassay ELISA kits according to the manufacturer's instructions. Briefly, the RAW264.7 cells (5×10^5 /well) [40] were plated on 6-well plates and treated with 1 μg/mL LPS prior to treatment with various conditions for 24 h. After 24 h incubation, the culture medium from each well was centrifuged at 2000 g for 10 min at 4 °C, and the supernatants were harvested for the determinations of PGE_2, TNF-α, IL-1β and IL-6. The concentrations of cytokines in the samples were calculated from standard curves. All of the experiments were performed in triplicate.

2.9.6. Quantitative RT-PCR

The mRNA expression levels of TNF-α, IL-1β, IL-6, COX-2 and iNOS in macrophages were measured by quantitative real-time PCR according to previously reported method [16]. The RAW264.7 cells (5×10^5 /well) were seeded in 6-well plates, cultured 12 h, and stimulated with 1 μg/mL LPS for 24 h before the treatment with various conditions for 24 h. The total RNA was extracted using RNAprep Pure Cell/Bacteria Kit (Tiangen Co., Ltd., Beijing, China) from the cells according to the manufacturer's instructions. The concentration and purity of the total RNA were determined by spectrophotometry (NanoDrop 2000, Thermo, USA) at 260/280 nm. Then, reverse transcription of total RNA into cDNA was performed using a reverse transcription kit (Tiangen Biotech (Beijing) Co., Ltd.). qRT-PCR was performed with the CFX96 Touch Real-Time PCR System (bio rad, USA) using PowerUp™ SYBR® Green Master Mix (ABI). The quantitative RT-PCR program was: 1 cycle at 95 °C for 10 s, 40 cycles at 95 °C for 5 s, followed by 55 °C for 15 s and 72 °C for 30 s. The primers for quantitative RT-PCR are listed in Table S3. The mRNA expression levels of iNOS, COX-2, TNF-α, IL-6, and IL-1β were quantified relative to the expression of β-actin as the endogenous control by the $2^{-\triangle\triangle CT}$ method.

2.9.7. Observation of morphological changes

The cells were washed with PBS three times and fixed with 10% formaldehyde in PBS for 1 h [41]. Then cells were washed twice with distilled water and stained with hematoxylin solution for 5 min at room temperature. Finally, wash once with distilled water and then the stained cells were visualized under the inverted fluorescence microscope.

2.10. Statistical analysis

All the experiments were carried out in triplicates. SPSS 11.0.0 statistical software (IBM, USA) was used for standard deviation calculations, pictures were done using GraphPad Prism 8.0.2 software.

3. Result and discussion

3.1. Single factor experiments

3.1.1. Entropy weighting method (EWM) and comprehensive evaluation value (CEV)

Multiple indicators influence the extraction or purification effect when facing the optimization of multiple ingredients, so the contents of these components are usually integrated into a CEV. Nowadays, the evaluation methods of comprehensive performance consist of percentage system, principal component analysis, grey correlation method or EWM [42], etc. In EWM, the objective weight of each indicator is assigned according to the degree of variation of various indicators. The greater the degree of variation of the index value, the more information it provides. Meanwhile, it plays greater role in the comprehensive evaluation and has greater weight [43]. By the EWM for determination entropy weight of FA and LIG, the result implied that 0.494 and 0.506 are FA and LIG entropy weight, respectively. The similar entropy weight

shows that FA and LIG had a virtually identical influence on the CEV, thereby FA and LIG are vital indicators of the quality of ASR [44]. Then, the CEV is obtained by the sum of the product of each indicator and its weight. Finally, CEV can be calculated by formula (4).

3.1.2. The effect of type and composition of the enzyme

The enzyme's ability to decompose the structure of the plant cell wall and the cell wall polysaccharides contributes to the target products extraction [45]. Moreover, the combination of two different enzymes will enhance the destructive effect [46]. Thus, in this study enzyme type and concentration were investigated. The results could be observed from Table S4 that the extraction yields of LIG and FA in the control sample (without any enzymatic treatment) were the lowest compared with any other positive pre-treatments. This phenomenon could be explained by the hydrolytic action of the mixed enzymes on the components of the cell wall and membrane [47]. Ultimately the plant cell wall of ASR became thinner and the microstructure was disorganized which facilitate the release of target product. Afterwards, Cel and Hem were chosen for the following experiments. The mixed enzymes concentration and ratio was studied and the result shown in Table S5, the highest CEV 4.35 were obtained by mixed enzyme treatment (Cel 160 U/g binding Hem 280 U/g). In addition, Cel and Hem can be made from agricultural waste, such as sorghum husk, wheat straw, sugarcane tops and leaves [48,49], which is in line with SDGs. Similarly, the effects of single enzyme concentration on extraction yields of FA and LIG, respectively, and the effects of mass fractions of $(NH_4)_2SO_4$ (%), mass fractions of ethanol (%), ultrasound power (W) and total extraction time (min) on extraction yields and CEV were shown in Fig. S1.

3.1.3. The effect of extraction pH and temperature

The effect of different pH and temperature of extraction were given in Fig. 1. Cel and Hem has been reported to be stable in the pH range of pH 4.0–6.0[50,51], and pH 3.5–5.5 was investigated in this study. Fig. 1 c shows that the CEV was pH-dependent, and reached a maximum value at pH 4.5, since pH does not only affect the enzyme activity, but also affects the solubility of FA and LIG. When pH increased to 5.0, the yields gradually decreased and the enzyme activity gradually declined that may because the pH value may stop enzyme activity by denaturing (altering) the three-dimensional shape of the enzyme by breaking ionic and hydrogen bonds [52]. So, we chose 4.5 as the best pH for the enzyme.

The results in Fig. 1 d demonstrated that the CEV increased with rising temperature, and reached the maximum yields at 35 °C. Enzymolysis temperature is a crucial parameter influencing the contents of FA and LIG. As shown in Fig. 1 d, the CEV increased in the temperature range from 30 °C to 35 °C and reached the highest CEV of 4.4, and then decreased with further increase in enzymolysis temperature. The main reason may be that 35 °C is the optimum hydrolysis temperature of Cel combined with Hem. If the temperature is too high, enzyme will lose its activity or LIG degrades gradually. LIG which is a very unstable compound degradation can be accelerated including photo-degradation, hydrolysis, oxidation and soon when the ambient temperature increased [12]. 35 °C was used as the extraction temperature in order to ensure enzyme activity and to protect the stability of the target products.

3.1.4. The effects of ultrasound time and liquid to materials ratio

The effect of different ultrasound time on CEV was shown in Fig. 1 e. Within a certain time range (10–30 min), the CEV gradually increased with ultrasound time rising, and decreased significantly between 30 and 90 min. The reason for this finding might be that stronger ultrasonic cavitation and the thermal effects arise by long ultrasound time may lead to degradation of FA and LIG. From the perspective of energy savings and practical production, 30 min will be selected as the ultrasound time.

The effect of different liquid to materials ratios on CEV is shown in Fig. 1 f. When the liquid to materials ratio was 25 mL/g, the CEV was lower and with the raising in the ratio, and at 35 mL/g, the CEV increased to a maximal value of 4.49.The increased liquid to materials ratios promoted the contact between the solvent and the raw materials, as well as the increased concentration gradient of target products inside and outside the cells will promote the dissolution of them [53]. Whereas when the liquid to materials ratio is too high, the enzyme concentration is significantly reduced that affects the enzymatic hydrolysis reaction. Thus, 35 mL/g will be chosen as the liquid to materials ratio.

Table 3
Analysis of variance (ANOVA) for response surface model of the CEV of extraction yield.

Source	Sum of squares	df	Mean square	F value	P-value	Significant [a]
Model	2.26	14	0.16	20.84	< 0.0001	***
X_1	0.16	1	0.16	20.47	0.0004	***
X_2	0.24	1	0.24	31.34	< 0.0001	***
X_3	0.091	1	0.091	11.79	0.0037	**
X_4	0.076	1	0.076	9.78	0.0069	**
X_1X_2	0.043	1	0.043	5.52	0.0329	*
X_1X_3	0.001076	1	0.001076	0.14	0.7148	–
X_1X_4	0.12	1	0.12	15.41	0.0014	**
X_2X_3	0.001617	1	0.001617	0.21	0.6545	–
X_2X_4	0.017	1	0.017	2.22	0.1565	–
X_3X_4	0.079	1	0.079	10.17	0.0061	**
X_1^2	0.041	1	0.041	5.24	0.0371	*
X_2^2	0.73	1	0.73	93.48	< 0.0001	***
X_3^2	0.64	1	0.64	82.69	< 0.0001	***
X_4^2	0.3	1	0.3	38.13	< 0.0001	***
Residual	0.12	15	0.007756			
Lack of fit	0.078	10	0.007837	1.03	0.5192	–
Pure error	0.038	5	0.007593			
Cor total	2.38	29				

a ***, most significant ($P < 0.001$); **, more significant ($P < 0.01$); *, significant ($P < 0.05$); -, less significant (P greater than 0.05).

3.2. Optimization of EUA-ATPE conditions with CCD

The results of the single factor experiment could be summarized as follows: ethanol, 25% (w/w) and $(NH_4)_2SO_4$, 18% (w/w); enzyme types and compositions, Cel (160 U/g) combined with Hem (280 U/g); the ultrasound power (700 W); total extraction time, 90 min; liquid to materials ratio of 35 mL/g; extraction temperature, 35 °C; ultrasound time, 30 min; and extraction pH of 4.5. Among these conditions, ATPS compositions chosen were in line with the pre-determined scales. The pH, temperature, liquid to materials ratio and ultrasound time in extraction were interrelated variables and needed further verification. As shown in Table 2, the central composite design (CCD), was introduced to determine the best combination of extraction variables for the CEV. As shown in Table 2, all experimental data were obtained from a 30-run-experiment by HPLC analysis (Fig. 1 b), the yield of FA ranged from 0.59 to 0.78 mg/g, the yield of LIG from 6.80 to 8.90 mg/g and CEV from 3.81 to 4.80. The results were fitted and the values of regression coefficients were calculated by the Design-Expert software version 10.0. To clarify the interaction of the four variables on the CEV, response surface plots

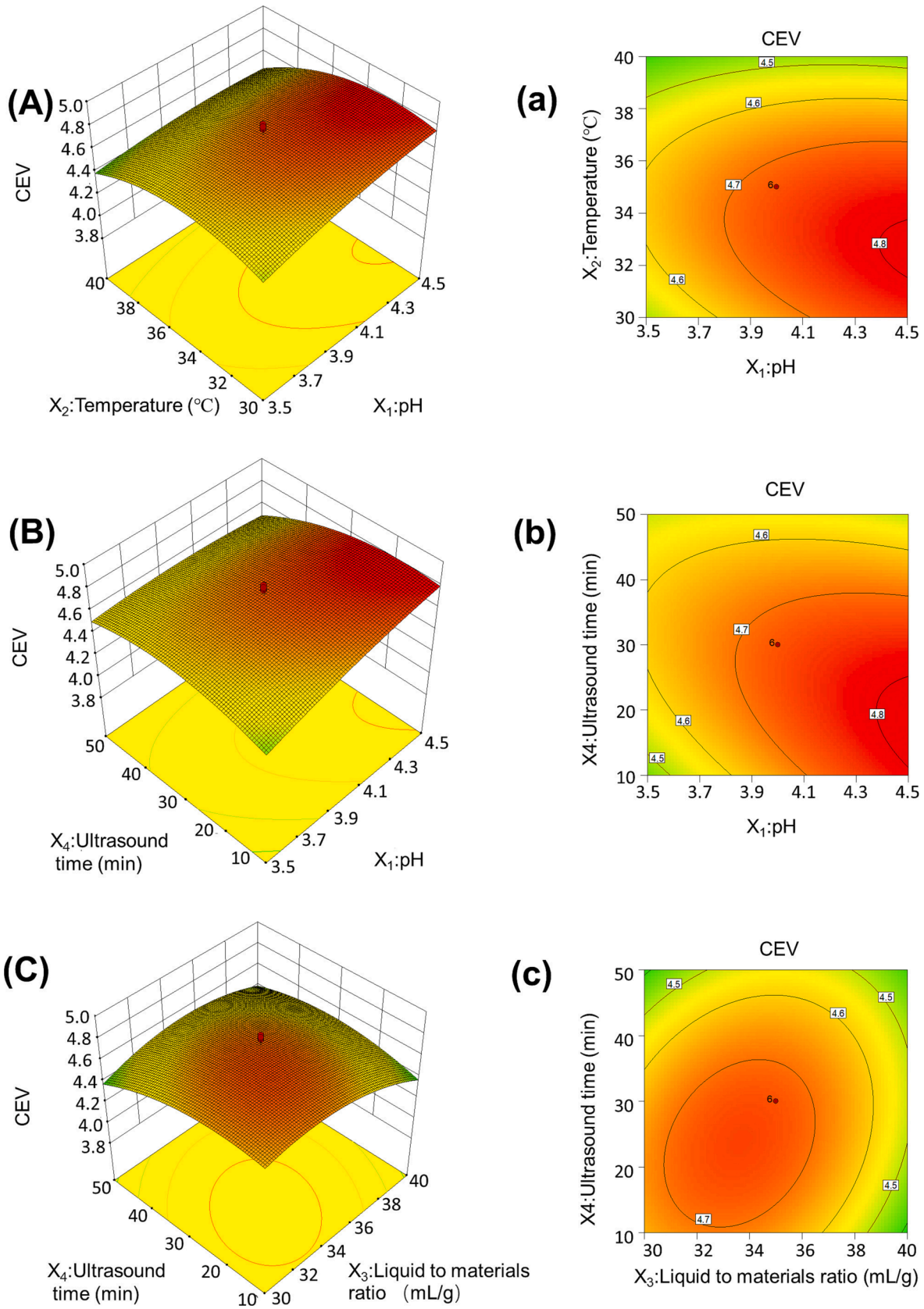

Fig. 3. Response surface plots (A-C) and contour plots (a-c) showing the effects of single factor on CEV. (A) and (a) Extraction temperature (℃) vs pH; (B) and (b) Ultrasound time (min)vs pH; (C) and (c) Ultrasound time (min) vs. ratio of liquid to solid (mL/g).

Table 4
The predicted and experimental results of the responses for FA and LIG under optimum conditions.

Yield (mg/g)					
FA	LIG	CEV	RSD (%)	CEV mean value[a]	Predicted
0.76	8.82	4.84	0.14	4.84 ± 0.0068	4.83
0.75	8.86	4.85			
0.75	8.83	4.84			
0.75	8.83	4.84			
0.75	8.82	4.83			

a Mean ± standard deviation (n = 5).

(A-C) and contour plots (a-c) were built. The response variable and the test variables are related by the following second-order polynomial equation:

$$Y = -16.60 + 2.49X_1 + 0.52X_2 + 0.42X_3 + 0.014X_4 - 0.021X_1X_2 - 3.28E-003X_1X_3 - 8.64E-003X_1X_4 - 4.02E-004X_2X_3 + 3.28E-004X_2X_4 + 7.02E-004X_3X_4 - 0.15X_1^2 - 6.46E-003X_2^2 - 6.08E-003X_3^2 - 3.09E-004X_4^2$$

The RSM model expressed in above equation has a correlation coefficient (R^2) of 0.9511 providing a trustworthy probe (as shown in Table 3) into factors and their interactions, which was not possible to identify using the single factor experiment. Among the four variables, X_1, X_2, X_3, and X_4, the linear coefficients (X_1, X_2), and the quadratic terms (X_2^2, X_3^2, X_4^2) were found significant ($p < 0.001$). As shown in Fig. 3 A, a, C and c, the composition variables, (X_1, X_2) and (X_3, X_4) interacted with each other since pH and ultrasound time may affect enzyme activity [54,55], and liquid to materials ratio and ultrasound time may affect the release and transfer of effective substances in the solvent. Hence, the CCD study was critical for the optimization of EUA-ATPE. The other interactions, although less significant in comparison with X_1X_4 (Fig. 3 B and b) were still relatively important and contributed to the CEV ($p < 0.05$). X_1, X_2, X_3 and X_4 were the most important variables from the process described above. Accordingly, the predicted values for CEV (4.83) were found in a response to our lab validation using $X_1 = 4.4$, $X_2 = 33$ °C, $X_3 = 35$ mL/g, and $X_4 = 25$ min. It was consistent with the values predicted in Table 4.

3.3. LC-MS/MS analysis

Table 5 shows a part of identified compounds from the LC-MS/MS analysis. Certain compounds, such as LIG, FA and senkyunolide H recorded similar findings with previous study [56-59]. Based on the biologically active substances in ASR, these compounds were sorted by the content. ASR has a number of pharmacological effects, such as adenosine, uridine and guanine, which have anti-platelet aggregation activity [60], and caffeic acid has blood-supplementing effect [61]. The total ion current chromatograms (TIC) of ASR extracts by EUA-ATPE in positive mode and negative mode can be obtained in Fig. S2.

3.4. Comparison of EUA-ATPE and different extraction methods

To demonstrate the effectiveness of EUA-ATPE in extraction, a series of comparative studies were performed. As shown in Table 6, higher yields of FA and LIG were obtained by EUA-ATPE instead of UA-ATPE, EA-ATPE and UAE, which indicated that the combination of ultrasonic and enzymatic hydrolysis can improve the extraction efficiency. On the one hand, enzymatic hydrolysis loosens the cell wall to release FA bound to the cell wall. On the other hand, the ultrasonication approach is more effective in destroying the external structure of the raw materials, allowing for better penetration of the solvent into the materials. SE is a classical method for extracting compounds from solid substances and is

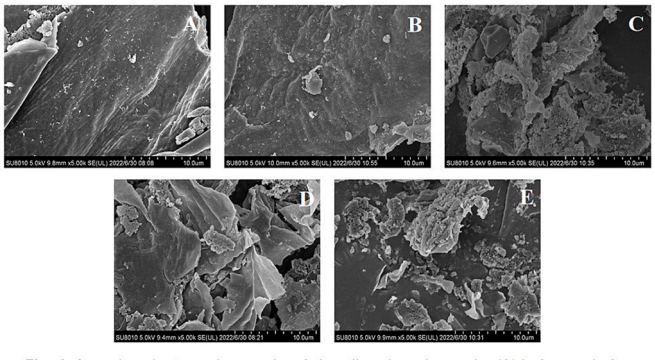

Fig. 4. Scanning electron micrographs of ASR powder (A) before and after extraction by (B)SE, (C)EA-ATPE, (D) UA-ATPE and (E) EUA-ATPE.

Table 5
The active compounds identified from EUA-ATPE extract sorted by the content.

No.	Compounds	Relative peak area value	RT (min)	Chemical formula	Molecular weight	Ion
1	Adenosine	483,700,000	2.76	$C_{10}H_{13}N_5O_4$	267.24	pos
2	Sodium ferulate	190,600,000	6.81	$C_{10}H_9NaO_4$	216.17	neg
3	Ligustilide	162,600,000	11.86	$C_{12}H_{14}O_2$	190.24	pos
4	Ferulic acid	154,000,000	6.88	$C_{10}H_{10}O_4$	194.19	neg
5	Uridine	57,280,000	1.86	$C_9H_{12}N_2O_6$	244.20	pos
6	Guanine	21,870,000	2.77	$C_5H_5N_5O$	151.13	neg
7	Caffeic acid	19,740,000	5.80	$C_9H_8O_4$	180.16	neg
8	3-Butylidenephthalide	7,174,000	11.83	$C_{12}H_{12}O_2$	188.22	pos
9	Senkyunolide H	1,913,000	9.50	$C_{12}H_{16}O_4$	224.26	pos
10	Vanillic acid	664,600	5.90	$C_8H_8O_4$	168.15	neg

Table 6
Extraction results of different extraction methods.

					FA			LIG			
Extraction methods	Solvent	Temperature (℃)	Time(min)	pH	K	R (%)	Y (mg/g)	K	R (%)	Y (mg/g)	CEV
UEA-ATPE	ATPS	35	ultrasound 25 + enzyme hydrolysis 65	4.5	2.87	79.69	0.72	201.99	99.63	8.71	4.76
UA-ATPE	ATPS	35	ultrasound 25 + water bath 65	7	2.12	74.22	0.53	152.89	99.52	6.80	3.71
EA-ATPE	ATPS	35	enzyme hydrolysis 90	4.5	2.16	74.71	0.57	163.26	99.55	7.28	3.96
SE	ethanol	70	water bath 90	–	–	–	0.52	–	–	8.00	4.30
UAE	ethanol	35	ultrasound 25	–	–	–	0.52	–	–	6.78	3.68

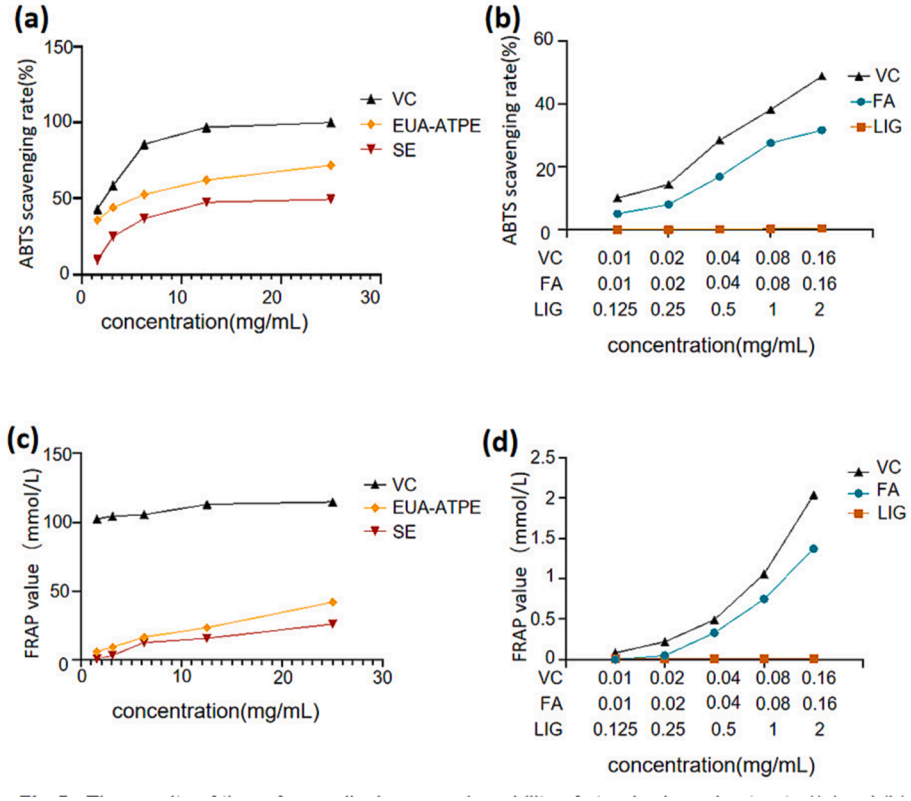

Fig. 5. The results of three free radical scavenging ability of standards and extracts ((a)and (b) ABTS) ((c)and (d) FRAP).

widely used for the extraction of natural products [62]. However, the EUA-ATPE method was more efficient than SE, and this method not only improve yield of target products but enhance energy efficiency. Besides, compared with SE, EUA-ATPE were less organic solvent consuming that coincide with green chemistry and SDGs. Thus, it was showed that the EUA-ATPE has the potential to be an efficient method for extracting phyto-bioactive chemicals and it was in line with environmentally friendly strategies.

Table 6 also shows the effects of the procedures on the recovery rates (R) and partition coefficient (K). The highest K of FA and LIG (2.87 and 201.99, respectively) were obtained by EUA-ATPE, with R of 79.69% and 99.63%. The lowest K of FA and LIG (2.12 and152.89, respectively) were obtained when extracted only by ultrasound assisted, with R of 74.22% and 99.52%, respectively. The K_{FA} and K_{LIG} were greater than 1 indicating that FA and LIG were preferentially partitioned to the hydrophilic ethanol-rich phase of the ATPS due to the hydrophobicity properties. The present findings suggests that alcohol/salt ATPS can serve to separate target product with high partition coefficient from natural sources [63]. Therefore, ATPE should be more widely used in hydrophobic substances' extraction.

3.5. SEM analysis

The microstructure can be observed by SEM imaging for exploration of the process mechanism. Accordingly, the morphological changes of the untreated ASR powder sample and samples treated by different extraction methods were shown in Fig. 4. Compared to the flat and smooth surface in the untreated sample, SE treated material exhibited slightly wrinkled (Fig. 4 A and B). A destruction on the external surface of plant' tissues of EA-ATPE treatments (Fig. 4 C) was detected. This treatment efficiency might be attribute to the synergistic effect Cel and Hem [13,46]. UA-ATPE image (Fig. 4 D) illustrated that the acoustic cavitation produced by the ultrasonic wave, which break the cell wall and cause cell tissue damage in different degrees, resulting in crack and rupture [64]. Relatively, EUA-ATPE (Fig. 4 E) damaged more cell tissue demonstrating the co-effect of EAE and UA-ATPE techniques. Although EAE would take longer time for enzymolysis reaction, the tissue deformation or rupture caused by UAE could accelerate this process [65]. Therefore, these results proved that EUA-ATPE was a rapid and efficient alternative to extraction of the FA and LIG.

3.6. Antioxidant capacity

Nowadays, the antioxidant ability of various natural sources has been studied in a big way [66,67]. The antioxidant capacity of the EUA-ATPE and SE extracts was examined using the ABTS scavenging activity and FRAP value test. As shown in Fig. 5 a and c, the scavenging rate of ABTS radicals and FRAP values of ascorbic acid (VC) showed a certain quantitative-effect relationship in a concentration range of 1.56–25 mg/mL. The scavenging rate of ABTS radicals and FRAP value treated by EUA-ATPE and SE extract also increased and then stabilized. Although EUA-ATPE extract antioxidant capacity was weaker than VC, it antioxidant capacity is better than SE extract. As shown in Fig. 5 b and d, the scavenging rate of ABTS and FRAP value treated with FA, LIG and VC in different concentration. The monomer concentrations of FA and LIG in Fig. 5 b and d were same as EUA-ATPE extract in Fig. 5 a and c in each point at same location. The antioxidant capacity of FA and VC increased with the increasing of concentration, but the antioxidant ability of FA is not as good as that of VC. The antioxidant potential of FA can be ascribed to its structural characteristics. Its potent antioxidant activity is explained by the formation of a resonance-stabilized phenoxy radical, because of its phenolic nucleus and an unsaturated side chain. The resonance stabilization accounts for the effective antioxidant potential of FA [68,69]. However, LIG has little antioxidant ability (Fig. 5 b and d), because it is belong to phthalide compound, but the antioxidant effect of volatile oil is mainly from alcohols, acids, phenolic, flavonoids and other compounds [70,71,73]. Thus antioxidant ability of ASR was mainly contribute to FA. To sum up EUA-ATPE not only improves the

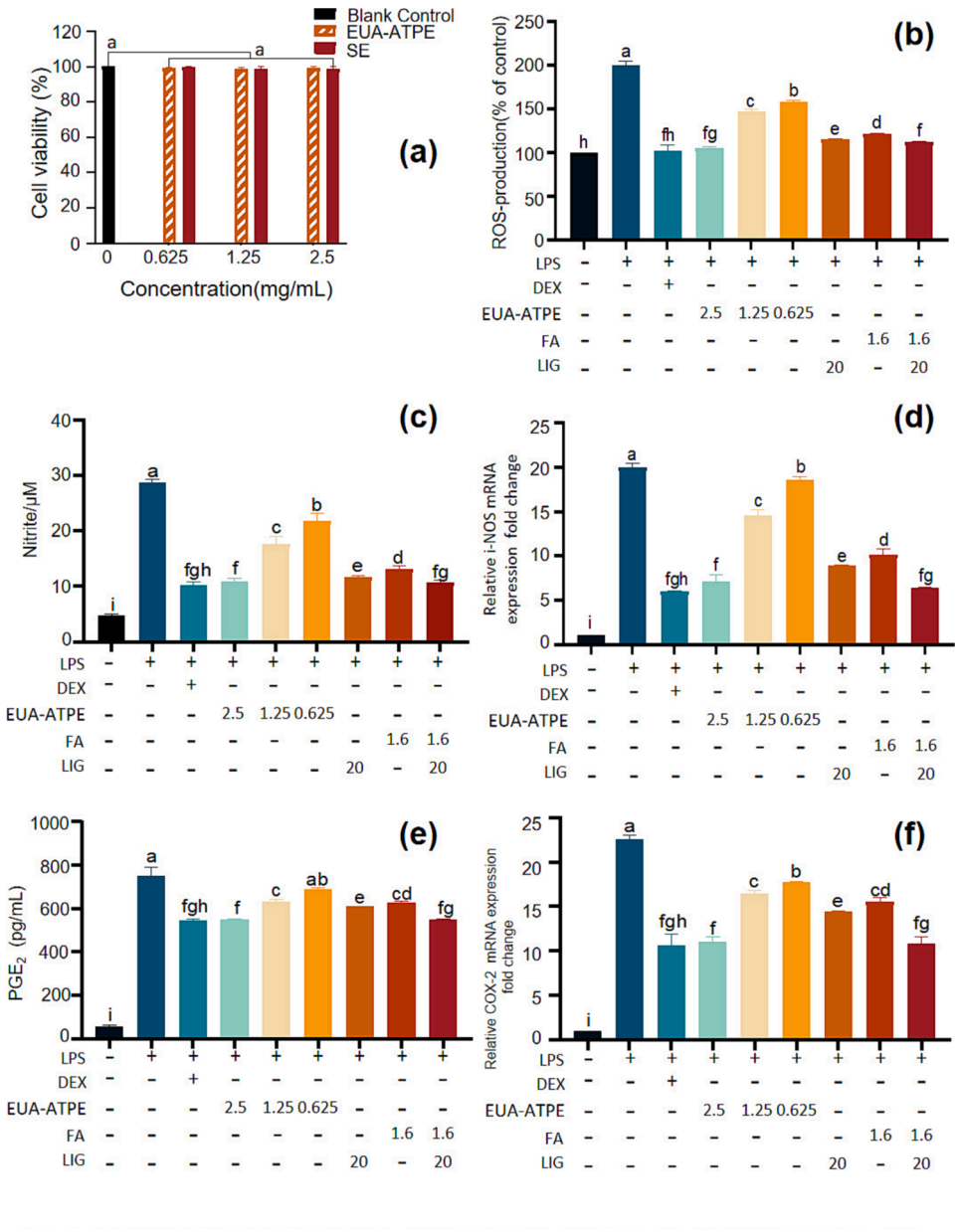

Fig. 6. (a) Cytotoxic effects of EUA-ATPE and SE extracts on RAW264.7 cells. (b) Intracellular ROS (iROS) production detected by DCF fluorescence. (c), The NO levels in the cell cultures were measured by Griess assays; (d) i-NOS mRNA expression, (e)The PGE_2 levels were measured by ELISA, (f) COX-2 mRNA expression. Cells were treated with LPS for 24 h and then incubated in different drugs 24 h. DEX: cells were treated with DEX at 1 μM; EUA-ATPE (2.5, 1.25 and 0.625): cells were treated with at concentrations range of 2.5, 1.25 and 0.625 mg/mL, respectively. FA: cells were treated with ferulic acid at concentrations 1.6 μg/mL. LIG: cells were treated with ligustilide at concentrations 20 μg/mL. The data represent the mean ± S.D. (n = 3). Different lowercase letters indicate significant differences ($P < 0.05$) in multiple-range analysis among the groups.

extraction rate of ASR, but improves the antioxidant capacity. So this method represents a promising alternative for the further investigation of extraction and enrichment of bioactive components.

3.7. *In vitro anti-inflammatory activity*

3.7.1. *Cell viability*

Effect of EUA-ATPE and SE extracts on the viability of RAW264.7 macrophages were evaluated. In this study, EUA-ATPE and SE had same mass concentration. As shown in Fig. 6 a, EUA-ATPE and SE extract at doses of 0.625–2.5 mg/mL had no effect (cell viability ≥ 90%) on the viability of RAW264.7 cells. The results suggested that EUA-ATPE and SE extracts were not cytotoxic to RAW264.7 cells at the above doses.

3.7.2. *Determination of intracellular reactive oxygen species (iROS) production*

LPS of continuation triggers uncontrolled production of inflammatory mediators, ultimately causing oxidative stress, inflammation, and high mortality rates especially in severe diseased state [72,73]. Numerous studies have shown that oxidative stress (e.g., ROS) is closely associated with the development of inflammation [74,75].Therefore to examine whether oxidative stress damage was involved in LPS-induced RAW264.7 macrophages inflammation, iROS levels were detected using DCFH-DA. As shown in Fig. 6 b, the iROS production in the LPS-stimulated group was significantly higher than that in the control group ($P < 0.05$). Compared with LPS group, treated cells with EUA-ATPE exacts reduced iROS generation in a concentration-dependent manner (0.625 to 2.5 mg/mL). The combination of FA and LIG (1.6 + 20 μg/mL) also could produce better anti-inflammation effect than FA (1.6 μg/mL) or LIG (20 μg/mL) alone. Moreover, 2.5 mg/mL EUA-ATPE extract and mixed monomer can restrain iROS level to DEX group level.

3.7.3. *Determination of NO and PGE_2 and the mRNA expression*

NO is an endogenous gaseous signal molecule, which can be produced as an inflammatory mediator in LPS-induced macrophages [76]. In the inflammatory response, NO is synthesized by iNOS [77]. Similar to NO, PGE_2 is response to inflammatory stimuli and it synthesized from arachidonic acid by COX-2 [78]. As shown in Fig. 6 c and e, the results

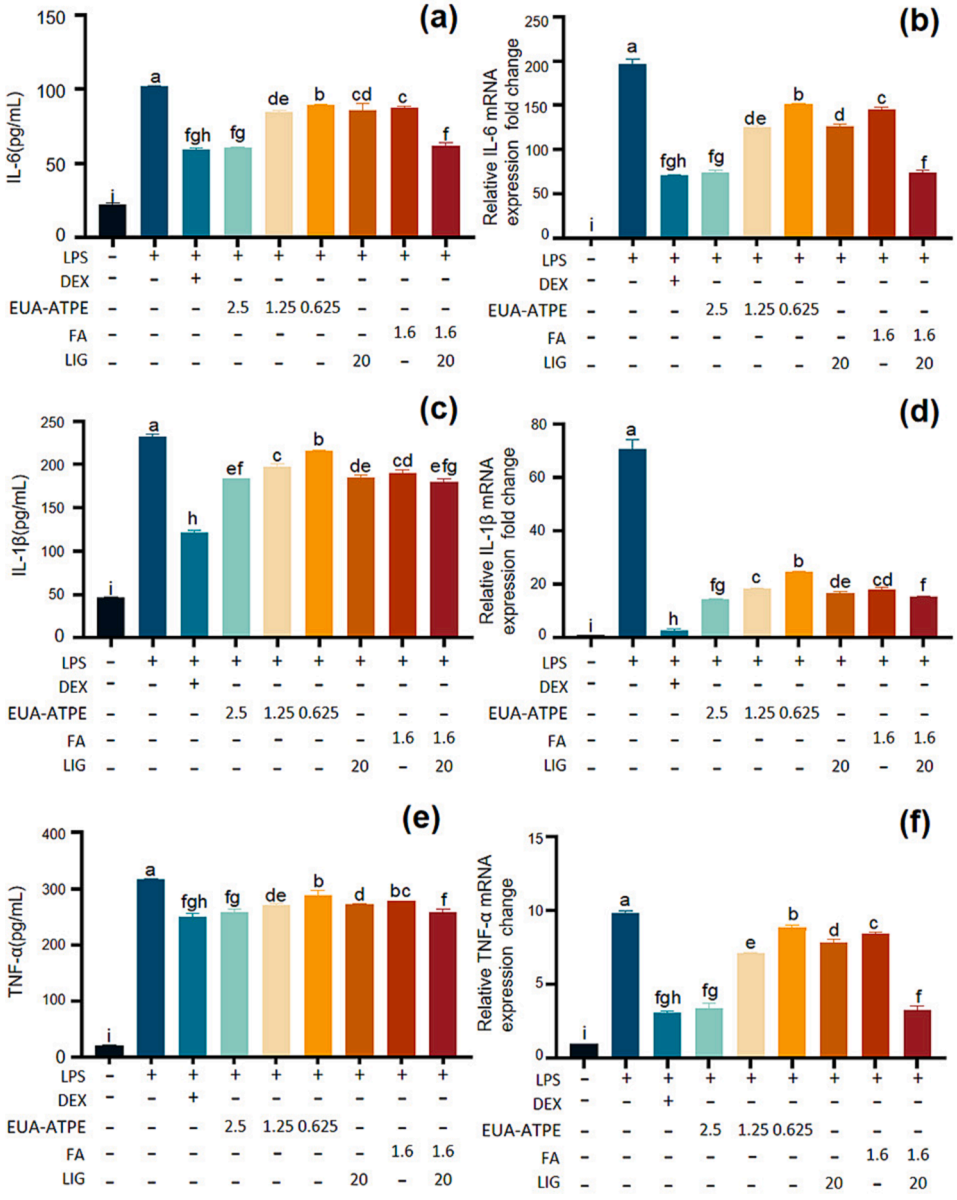

Fig. 7. (a) Proinflammatory cytokines IL-6, (c) IL-1β and (e) TNF-α secretion in LPS induced RAW264.7 cells. (b) IL-6 and, (d) IL-1β, (f) TNF-α mRNA expression. Cells were treated with LPS for 24 h and then incubated different drugs 24 h. DEX: cells were treated with DEX at 1 μM; EUA-ATPE (2.5, 1.25 and 0.625): cells were treated with at concentrations range of 2.5, 1.25 and 0.625 mg/mL, respectively. FA: cells were treated with ferulic acid at concentrations 1.6 μg/mL. LIG: cells were treated with ligustilide at concentrations 20 μg/mL. The data represent the mean ± S.D. (n = 3). Different lowercase letters indicate significant differences ($P < 0.05$) in multiple-range analysis among the groups.

showed that LPS induced significantly increased NO and PGE_2 production, compared with untreated LPS group. EUA-ATPE extracts reduced NO and PGE_2 production in a dose-dependent manner in concentration from 0.625 to 2.5 mg/mL. The combination of FA and LIG (1.6 + 20 μg/mL) also could reduce NO and PGE_2 production apparently than FA (1.6 μg/mL) or LIG (20 μg/mL) alone. Furthermore, 2.5 mg/mL EUA-ATPE extract and mixed monomer can suppress NO and PGE_2 level to DEX group degree.

In the inflammatory response, NO and PGE_2 are synthesized by iNOS and COX-2, respectively [48]. To confirm whether the suppression of NO and PGE_2 production were related to changes in iNOS as well as COX-2 mRNA levels, qRT-PCR was performed. Fig. 6 d and f showed that iNOS and COX-2 mRNA expression was increased in LPS induced cells. At the same time, pretreated EUA-ATPE extracts significantly decreased the expression of iNOS and COX-2 mRNA levels in a concentration-dependent manner from 0.625 to 2.5 mg/mL. The combination of FA and LIG (1.6 + 20 μg/mL) reduced iNOS and COX-2 mRNA levels as well, which was more than FA (1.6 μg/mL) or LIG (20 μg/mL). Moreover, 2.5 mg/mL EUA-ATPE extract and mixed monomer group restrain iNOS and COX-2 mRNA levels to DEX group level. These findings indicate that FA combined LIG has inhibitory effect on LPS-induced NO and PGE_2 generation in RAW264.7 cells by suppressing iNOS and COX-2 mRNA expression. Thus, FA and LIG in EUA-ATPE extract might play an essential role in ameliorating inflammation by suppressing NO and PGE_2 production and downregulation of iNOS and COX-2 mRNA expression.

3.7.4. Determination of proinflammatory cytokines and the mRNA expression

Macrophages will release inflammatory cytokines during cellular immunity which is an important aspect of maintaining immune regulation [79]. In order to confirm the anti-inflammatory activity of the EUA-ATPE extract, the effects of the extract on proinflammatory cytokines (IL-6, IL-1β and TNF-α) production were evaluated in LPS induced RAW264.7 cells by ELISA. As presented in Fig. 7 a, c and e, LPS treatment resulted in a significantly increased releases of IL-6, IL-1β, TNF-α compared to untreated LPS cells. As shown in Fig. 7, as expected, DEX could inhibit LPS induced IL-6, IL-1β and TNF-α production and downregulate corresponding mRNA expression, respectively. EUA-ATPE extracts inhibited proinflammatory cytokines (IL-6, IL-1β and TNF-α) secretion in a dose dependent manner in a concentration-dependent

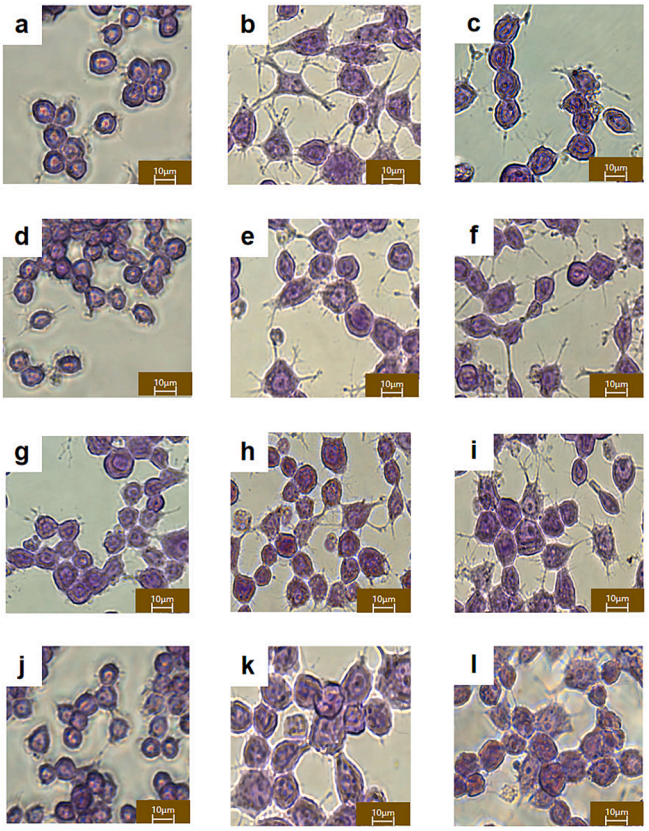

Fig. 8. Morphological change in macrophage RAW264.7 cells. Cells were stained with hematoxylin staining. Morphology of macrophage RAW264.7 cells visualized by optical microscopy (original magnification at × 400, scale bar; 10 μm). The cells were pretreated with LPS for 24 h and then incubation with (a) Control, (b) LPS- (1 μg /mL) treated only, (c) cells were treated with DEX at 1 μM, (d), (e) and (f) cells were treated with EUA-ATPE extract at concentrations of 2.5, 1.25, and 0.625 mg/mL, respectively, (g), (h) and (i) cells were treated with SE extract at concentrations of 2.5, 1.25, and 0.625 mg/mL, respectively. (j) monomer mixture-treated, (k) LIG, (I) FA.

manner from 0.625 to 2.5 mg/mL. The qRT-PCR was performed to investigate whether suppression of IL-6, IL-1β and TNF-α production by different treated was related to a change in mRNA levels of three proinflammatory cytokines. As shown in Fig. 7 b, d and f, increasing concentrations of EUA-ATPE extracts produced a decrease gradually in IL-6, IL-1β and TNF-α mRNA levels, respectively. The mixture of FA and LIG (1.6 + 20 μg/mL) also could lessen secretion of proinflammatory cytokines and proinflammatory mRNA expression than FA (1.6 μg/mL) or LIG (20 μg/mL). In brief, FA and LIG in EUA-ATPE extract might play an important role in ameliorating inflammation.

In order to confirm the anti-inflammatory activity of the EUA-ATPE and SE extracts, iROS, NO, PGE_2, proinflammatory cytokines (IL-6, IL-1β and TNF-α) production and corresponding mRNA expression were evaluated in LPS induced RAW264.7 cells. The result showed (Fig. S3 and Fig. S4) that inflammatory mediator, proinflammatory cytokines and mRNA level were higher in RAW264.7 cells treated with SE extract (0.625–2.5 mg/mL) than those treated with EUA-ATPE (0.625–2.5 mg/mL) in same concentration.

3.7.5. Morphology of macrophage RAW264.7 cells

The effect of EUA-ATPE and SE extracts on cell morphology was detected using the optical microscope. As depicted in Fig. 8 a, the normal morphology of RAW264.7 cell was round, and the cell boundary was clear. The results demonstrated that LPS caused cell morphology to change into a pseudopodia formation, spreading, and pancake-like shape within 24 h of stimulation (Fig. 8 b) and DEX group shown a little change in cell morphology (Fig. 8 c). The morphological alteration in the presence of EUA-ATPE extract and SE extract in different concentration were observed in Fig. 8 d-i. The pretreatment with EUA-ATPE and SE extracts decreased the degree of cell spreading and pseudopodia formation in varying degrees, which were observed that cells morphology changed were more apparent in same concentration (0.625–2.5 mg/mL) treated with SE extract. As shown in Fig. 8 k, l and j, compared with FA and LIG groups, the cell morphology changed less in monomer mixture-treated group which degree of morphological change was similar to DEX treated group. Similar to our study, extract of Citrus aurantium L. has an anti-inflammatory effect on LPS-induced RAW264.7 cells, and reduced the level of cell spreading and pseudopodia formation on cell morphology can be seen [80]. Macrophage activation is the most essential phase of the immune response. The most intuitive feature of macrophage activation would be the alteration of cell morphology such as changing to an irregular form with accelerated spreading and forming pseudopodia [81]. However, anti-inflammation medicine can restrain this morphology changes.

4. Conclusion

In this study, the single factor experiments and CCD were employed to optimize extraction conditions. With the APTS of $(NH_4)_2SO_4$-ethanol system as the biphasic extractant, both FA and LIG achieved the maximum extraction yields of 0.78 mg/g and 8.9 mg/g, respectively, and CEV reached 4.80 under the optimum conditions. The microcosmic surface of ASR powder observed by SEM illustrated that the synergistic effect combined EAE with UA-ATPE was facilitated to plant cell wall rupture and enzymolysis compared with SE, UA-ATPE and EA-ATPE, improving the extraction yields ultimately. Furthermore, antioxidant activity assays showed that ASR extracts by EUA-ATPE had stronger scavenging ability to ABTS radicals and FRAP value then by SE. Whereas, paralleled with FA, LIG had little antioxidant activity in vitro. ASR extracts by EUA-ATPE, FA and LIG exerted an antioxidative effect and anti-inflammatory effects by suppressing both proinflammatory mediators and relevant gene expression in LPS induced RAW264.7 cells. Hence, EUA-ATPE integrating EAE with UA-ATPE in a one-step procedure provided a highly efficient approach to extract of FA and LIG from ASR simultaneously.

In conclusion, the innovative techniques integrated enzymatic hydrolysis, ultrasound and aqueous two-phase extraction has achieved satisfactory results, which can be appropriate alternatives to conventional methods for the extraction of ASR bio-actives, since it is higher production compared with the conventional ones. Besides EUA-ATPE method provides a green procedure which had less organic solvent and energy consuming that thereby aligning with SDGs. Therefore, this innovative and sustainable extraction process can provide new thoughts for other plant extraction.

Author contributions

Yan-Hua Li and Yan-Yan Liu designed the whole experiment; Xue-Jiao Song directed the completion of the experiment; Chang Liu, Yang Zhang, Xiao-Xue Xiao, Guo-Rui Han, Ke-Di Sun, Shuo-Qi Liu, Zhi-Yun Zhang, Chun-Liu Dong, Ya-Dan Zheng, Xue-Ying Chen and Tong Xu were supportive during the experiment.

Declaration of Competing Interest

The authors declare that they have no known competing financial interests or personal relationships that could have appeared to influence the work reported in this paper.

Data availability

Data will be made available on request.

Acknowledgments

This work was supported by National Nature Science Foundation of China (Grant No. 32072908), the China Agriculture Research System of MOF and MARA and the Key Research and Development Program of Heilongjiang Province (Grant No.GA21B006).

Appendix A. Supplementary data

Supplementary data to this article can be found online at https://doi.org/10.1016/j.ultsonch.2023.106344.

References

[1] U. Nations, Transforming Our World: The 2030 Agenda for Sustainable Development, in, 2023.
[2] C. Lu, M. Liu, W. Shang, Y. Yuan, K. Yang, Knowledge Mapping of Angelica sinensis (Oliv.) Diels (Danggui) Research: A Scientometric Study, Front. Pharmacol. 11 (2020).
[3] C.-Y. Cheng, S.-T. Kao, Y.-C. Lee, Angelica sinensis extract protects against ischemia-reperfusion injury in the hippocampus by activating p38 MAPK-mediated p90RSK/p-Bad and p90RSK/CREB/BDNF signaling after transient global cerebral ischemia in rats, J. Ethnopharmacol. 252 (2020).
[4] F. Cheng, Y. Zhang, Q. Li, F. Zeng, K. Wang, Inhibition of Dextran Sodium Sulfate-Induced Experimental Colitis in Mice by Angelica Sinensis Polysaccharide, J. Med. Food 23 (2020) 584–592.
[5] L.i. Jian, H.a. Yongli, J.i. Peng, Y. Wanling, Z. Haifu, Effects of volatile oils of Angelica sinensis on an acute inflammation rat model, Pharm. Biol. 54 (2016) 1881–1890.
[6] Z. Wen-quan, Yong-li, Hua, Man, Zhang, Peng, Ji, Jin-xia, Li, Metabonomic analysis of the anti-inflammatory effects of volatile oils ofAngelica sinensison rat model of acute inflammation, Biomed. Chromatogr. 29 (2014).
[7] J. Li, Y. Hua, P. Ji, W. Yao, H. Zhao, L. Zhong, Y. Wei, Effects of volatile oils of Angelica sinensis on an acute inflammation rat model, Pharm. Biol. 54 (2016) 1881–1890.
[8] Y. Long, D. Li, S. Yu, A. Shi, J. Deng, J. Wen, X.-Q. Li, Y. Ma, Y.-L. Zhang, S.-Y. Liu, J.-Y. Wan, N. Li, M. Yang, L. Han, Medicine–food herb: Angelica sinensis, a potential therapeutic hope for Alzheimer's disease and related complications, Food Funct. (2022).
[9] J.W. Chung, R.J. Choi, E.K. Seo, J.W. Nam, M.S. Dong, E.M. Shin, L.Y. Guo, Y. S. Kim, Anti-inflammatory effects of (Z)-ligustilide through suppression of mitogen-activated protein kinases and nuclear factor-κB activation pathways, Arch. Pharm. Res. 35 (2012) 723–732.
[10] Y. Huang, Y. Zhang, T. Wan, Y. Mei, Z. Wang, J. Xue, Y. Luo, M. Li, S. Fang, H. Pan, Q. Wang, J. Fang, Systems pharmacology approach uncovers Ligustilide attenuates experimental colitis in mice by inhibiting PPAR gamma-mediated inflammation pathways, Cell Biol. Toxicol. 37 (2021) 113–128.
[11] Y. Li, J. Huang, Z. Hu, M. Zeng, Z. Liu, Y. Hu, Host–guest stoichiometry affects the physicochemical properties of beta-cyclodextrin/ferulic acid inclusion complexes and films, Food Funct. 13 (2022).
[12] F. Cui, L. Feng, J. Hu, Factors affecting stability of z-ligustilide in the volatile oil of radix angelicae sinensis and ligusticum chuanxiong and its stability prediction, Drug Dev. Ind. Pharm. 32 (2006) 747–755.
[13] M.M.A. Rashed, Q. Tong, A. Nagi, J. Li, N.U. Khan, L. Chen, A. Rotail, A.M. Bakry, Isolation of essential oil from Lavandula angustifolia by using ultrasonic-microwave assisted method preceded by enzymolysis treatment, and assessment of its biological activities, Ind. Crop. Prod. 100 (2017).
[14] S.V. Pawar, V.K. Rathod, Ultrasound assisted process intensification of uricase and alkaline protease enzyme co-production in Bacillus licheniformis, Ultrason. Sonochem. 45 (2018).
[15] C. Xing, W.-Q. Cui, Y. Zhang, X.-S. Zou, J.-Y. Hao, S.-D. Zheng, T.-T. Wang, X.-Z. Wang, T. Wu, Y.-Y. Liu, X.-Y. Chen, S.-G. Yuan, Z.-Y. Zhang, Y.-H. Li, Ultrasound-assisted deep eutectic solvents extraction of glabridin and isoliquiritigenin from Glycyrrhiza glabra: Optimization, extraction mechanism and in vitro bioactivities, Ultrason. Sonochem. 83 (2022).
[16] X.-Z. Wang, X.-J. Song, C. Liu, et al., Active components and molecular mechanism of Syringa oblata Lindl. in the treatment of endometritis based on pharmacology network prediction[J], Front. Vet. Sci. (2022) 9.
[17] C. Picot-Allain, M.F. Mahomoodally, G. Ak, G. Zengin, Conventional versus green extraction techniques - a comparative perspective, Current Opinion in Food, Science 40 (2021) 144–156.
[18] H.C. Nguyen, H.N.T. Nguyen, M.Y. Huang, K.H. Lin, D.C. Pham, Y.B. Tran, C.H. Su, Optimization of aqueous enzyme-assisted extraction of rosmarinic acid from rosemary (Rosmarinus officinalis L.) leaves and the antioxidant activity of the extract, J. Food Process. Preserv. 45 (2021).
[19] J.-A. Lin, C.-H. Kuo, B.-Y. Chen, Y. Li, Y.-C. Liu, J.-H. Chen, C.-J. Shieh, A novel enzyme-assisted ultrasonic approach for highly efficient extraction of resveratrol from Polygonum cuspidatum, Ultrasonics - Sonochemistry 32 (2016).
[20] N. Wan, P. Kou, H.-Y. Pang, Y.-H. Chang, L. Cao, C. Liu, C.-J. Zhao, C.-B. Gu, Y.-J. Fu, Enzyme pretreatment combined with ultrasonic-microwave-assisted surfactant for simultaneous extraction of essential oil and flavonoids from Baeckea frutescens, Ind. Crop. Prod. 174 (2021).
[21] J.L. Luque-Garcia, L. De Castro, Ultrasound: a powerful tool for leaching[J], Trac-Trends Anal. Chem. 22 (1) (2003) 41–47.
[22] P. Li, H. Xue, M. Xiao, J. Tang, H. Yu, Y. Su, X. Cai, Ultrasonic-Assisted Aqueous Two-Phase Extraction and Properties of Water-Soluble Polysaccharides from Malus hupehensis, Molecules 26 (2021).
[23] X.Q. Fu, G.L. Zhang, L. Deng, Y.Y. Dang, Simultaneous extraction and enrichment of polyphenol and lutein from marigold (Tagetes erecta L.) flower by an enzyme-assisted ethanol/ammonium sulfate system, Food Funct. (2019).
[24] Y. Lin, J. Pi, P. Jin, Y. Liu, X. Mai, P. Li, H. Fan, Enzyme and microwave co-assisted extraction, structural characterization and antioxidant activity of polysaccharides from Purple-heart Radish, Food Chem. 372 (2022).
[25] R.M. Banik, D.K. Pandey, Optimizing conditions for oleanolic acid extraction from Lantana camara roots using response surface methodology, Ind. Crop. Prod. 27 (2008) 241–248.
[26] Y. Liu, S. Wei, M. Liao, Optimization of ultrasonic extraction of phenolic compounds from Euryale ferox seed shells using response surface methodology, Ind. Crop. Prod. 49 (2013) 837–843.
[27] A. Asfaram, M. Ghaedi, H. Javadian, A. Goudarzi, Cu- and S- @SnO2 nanoparticles loaded on activated carbon for efficient ultrasound assisted dispersive mu SPE-spectrophotometric detection of quercetin in Nasturtium officinale extract and fruit juice samples: CCD-RSM design, Ultrason. Sonochem. 47 (2018) 1–9.
[28] Z. Cheng, H. Song, Y. Zhang, D. Han, X. Yu, Q. Shen, F. Zhong, Concurrent Extraction and Purification of Gentiopicroside from Gentiana scabra Bunge Using Microwave-Assisted Ethanol-Salt Aqueous Two-Phase Systems, J. Chromatogr. Sci. 58 (2019) 60–74.
[29] Z. Cheng, H. Song, X. Cao, Q. Shen, D. Han, F. Zhong, H. Hu, Y. Yang, Simultaneous extraction and purification of polysaccharides from Gentiana scabra Bunge by microwave-assisted ethanol-salt aqueous two-phase system, Ind. Crop. Prod. 102 (2017).
[30] M. Chouaibi, L. Rezig, S. Hamdi, G. Ferrari, Chemical characteristics and compositions of red pepper seed oils extracted by different methods, Ind. Crop. Prod. 128 (2019) 363–370.
[31] Z. Wang, P. Yang, H. Peng, C. Li, C. Yue, W. Li, X. Jiang, Comprehensive evaluation of 47 tea Camellia sinensis (L.) O. Kuntze germplasm based on entropy weight method and grey relational degree, Genet. Resour. Crop Evol. 68 (2021) 3257–3270.
[32] Y. Du, P. Huang, W. Jin, C. Li, J. Yang, H. Wan, Y. He, Optimization of Extraction or Purification Process of Multiple Components from Natural Products: Entropy Weight Method Combined with Plackett-Burman Design and Central Composite Design, Molecules 26 (2021).
[33] X.Q. Fu, M. Na, W.P. Sun, Y.Y. Dang, Microwave and enzyme co-assisted aqueous two-phase extraction of polyphenol and lutein from marigold (Tagetes erecta L.) flower, Ind. Crop. Prod. 123 (2018) 296–302.
[34] B. Qin, X. Liu, H. Cui, et al., Aqueous two-phase assisted by ultrasound for the extraction of anthocyanins from Lycium ruthenicum Murr[J], Prep. Biochem. Biotechnol. 47 (9) (2017) 881–888.
[35] C. Mca, C. Lr, C. Sh, B. Gfa, Chemical characteristics and compositions of red pepper seed oils extracted by different methods - ScienceDirect, Ind. Crop. Prod. 128 (2019) 363–370.
[36] W. Wu, S. Jiang, M. Liu, S. Tian, Simultaneous process optimization of ultrasound-assisted extraction of polyphenols and ellagic acid from pomegranate (Punica granatum L.) flowers and its biological activities, Ultrason. Sonochem. 80 (2021).
[37] C. Zhao, T. Xia, D. Peng, W. Duan, Y. Yu, Chemical Composition and Antioxidant Characteristic of Traditional and Industrial Zhenjiang Aromatic Vinegars during the Aging Process, Molecules 23 (2018) 2949.
[38] Q. Lin, Q. Liang, C. Qin, et al., CircANKRD36 Knockdown Suppressed Cell Viability and Migration of LPS-Stimulated RAW264.7 Cells by Sponging MiR-330[J], Inflammation 44 (5) (2021) 2044–2053.
[39] T. Jiang, J. Zhou, W. Liu, W. Tao, Y. Li, The anti-inflammatory potential of protein-bound anthocyanin compounds from purple sweet potato in LPS-induced RAW264.7 macrophages, Food Res. Int. 137 (2020), 109647.
[40] W. Peng, X. Minhao, C. Guijie, D. Zhuqing, H.u. Bing, Anti-inflammatory effects of dicaffeoylquinic acids from Ilex kudingcha on lipopolysaccharide-treated RAW264.7 macrophages and potential mechanisms, Food Chem. Toxicol. (2019).
[41] B. Dunkhunthod, K. Thumanu, G. Eumkeb, Application of FTIR microspectroscopy for monitoring and discrimination of the anti-adipogenesis activity of baicalein in 3T3-L1 adipocytes[J], Vib. Spectrosc. 89 (2017) 92–101.
[42] X. Wang, H. Wang, K. Hu, Y. Li, T. Qin, W. Zeng, X. Li, K. Zhang, J. Zhang, J. Bai, Comprehensive Evaluation of Introduced Potato Germplasms Resources Based on the Analytical Hierarchy Process and GGE-biplot, J. Plant Genetic Resour. 18 (2017) 1067–1078.
[43] Z. Wang, P. Yang, H. Peng, C. Li, X. Jiang, Comprehensive evaluation of 47 tea [Camellia sinensis (L.) O. Kuntze] germplasm based on entropy weight method and grey relational degree, Genet. Resour. Crop Evol. (2021).
[44] Z.-Y. Zhang, Y.-J. Wang, H. Yan, X.-W. Chang, G.-S. Zhou, L. Zhu, P. Liu, S. Guo, T. T.X. Dong, J.-A. Duan, Rapid Geographical Origin Identification and Quality Assessment of Angelicae Sinensis Radix by FT-NIR Spectroscopy, J. Anal. Methods Chem. 2021 (2021).
[45] M.M.A. Rashed, Q.Y. Tong, A. Nagi, J.P. Li, N.U. Khan, L. Chen, A. Rotail, A. M. Bakry, Isolation of essential oil from Lavandula angustifolia by using ultrasonic-microwave assisted method preceded by enzymolysis treatment, and assessment of its biological activities, Ind. Crop. Prod. 100 (2017) 236–245.
[46] K. Hosni, I. Hassen, H. Chaabane, M. Jemli, S. Dallali, H. Sebei, H. Casabianca, Enzyme-assisted extraction of essential oils from thyme (Thymus capitatus L.) and rosemary (Rosmarinus officinalis L.): Impact on yield, chemical composition and antimicrobial activity, Ind. Crop. Prod. 47 (2013) 291–299.

[47] X.-G. Zhang, Y. Lu, W.-N. Wang, Z.-Y. Liu, J.-W. Liu, X.-Q. Chen, A novel enzyme-assisted approach for efficient extraction of Z-ligustilide from Angelica sinensis plants, Sci. Rep. 7 (2017).
[48] S.D. Kshirsagar, B.N. Bhalkar, P.R. Waghmare, G.D. Saratale, R.G. Saratale, S. P. Govindwar, Sorghum husk biomass as a potential substrate for production of cellulolytic and xylanolytic enzymes by Nocardiopsis sp KNU, 3, Biotech 7 (2017).
[49] P. Dey, S. Chakrabortty, D. Haldar, V. Rangarajan, S. Ashok, On-site enriched production of cellulase enzyme using rice straw waste and its hydrolytic performance evaluation through systematic dynamic modeling, Environ. Sci. Pollut. Res. Int. (2022).
[50] J.-J. Yuan, C.-Z. Wang, J.-Z. Ye, R. Tao, Y.-S. Zhang, Enzymatic Hydrolysis of Oleuropein from Olea europea (Olive) Leaf Extract and Antioxidant Activities, Molecules 20 (2015) 2903–2921.
[51] Y. Jiang, Y. Ding, D. Wang, Y. Deng, Y. Zhao, Radio frequency-assisted enzymatic extraction of anthocyanins from Akebia trifoliata (Thunb.) Koidz. flowers: Process optimization, structure, and bioactivity determination, Ind. Crop. Prod. 149 (2020).
[52] Z. Li, X. Wang, G. Shi, Y. Bo, X. Lu, X. Li, R. Shang, L. Tao, J. Liang, Enzyme-assisted extraction of naphthodianthrones from Hypericum perforatum L. by 12C6 +-ion beam-improved cellulases, Sep. Purif. Technol. 86 (2012) 234–241.
[53] L. Zhang, J.Y. Mei, M.H. Ren, Z. Fu, Optimization of enzyme-assisted preparation and characterization of Arenga pinnata resistant starch, Food Struct. 25 (2020).
[54] Z. Wang, X. Lin, P. Li, Z. Jie, S. Wang, H. Ma, Effects of low intensity ultrasound on cellulase pretreatment, Bioresour. Technol. 117 (2012) 222–227.
[55] Y.-J. Fu, W. Liu, Y.-G. Zu, et al., Enzyme assisted extraction of luteolin and apigenin from pigeonpea Cajanus cajan (L.) Millsp. leaves[J], Food Chem. 111 (2) (2008) 508–512.
[56] L. Yi, Y. Liang, H. Wu, D. Yuan, The analysis of Radix Angelicae Sinensis (Danggui), J. Chromatogr. A 1216 (2009) 1991–2001.
[57] L. Wang, S. Huang, B. Chen, X.Y. Zang, D. Su, J. Liang, F. Xu, G.X. Liu, M.Y. Shang, S.Q. Cai, Characterization of the Anticoagulative Constituents of Angelicae Sinensis Radix and Their Metabolites in Rats by HPLC-DAD-ESI-IT-TOF-MSn, Planta Med. 362–370 (2016).
[58] J.-L. Lü, J.A. Duan, Y.P. Tang, N.Y. Yang, L.B. Zhang, Phthalide mono- and dimers from the radix of Angelica sinensis, Biochem. Syst. Ecol. 37 (2009) 405–411.
[59] Z.B. Dong, S.P. Li, M. Hong, Q. Zhu, Hypothesis of potential active components in Angelica sinensis by using biomembrane extraction and high performance liquid chromatography, J. Pharm. Biomed. Anal. 38 (2005) 664–669.
[60] K. Zhang, X. Shen, L. Yang, Q. Chen, N. Wang, Y. Li, P. Song, M. Jiang, G. Bai, P. Yang, Z. Yang, Exploring the Q-markers of Angelica sinensis (Oliv.) Diels of anti-platelet aggregation activity based on spectrum-effect relationships, Biomed. Chromatogr. 36 (2022).
[61] P. Ji, C. Li, Y. Wei, F. Wu, S. Liu, Y. Hua, W. Yao, X. Zhang, Z. Yuan, Y. Wen, Screening study of blood-supplementing active components in water decoction of Angelica sinensis processed with yellow rice wine based on response surface methodology, Pharm. Biol. 58 (2020) 1167–1176.
[62] S. Nuchdang, N. Phruetthinan, P. Paleeleam, V. Domrongpokkaphan, S. Chuetor, P. Chirathivat, C. Phalakornkule, Soxhlet, microwave-assisted, and room temperature liquid extraction of oil and bioactive compounds from palm kernel cake using isopropanol as solvent, Ind. Crop. Prod. 176 (2022).
[63] S.N. Hui, P.E. Kee, H.S. Yim, J.S. Tan, H.C. Yin, C.W. Lan, Characterization of alcohol/salt aqueous two-phase system for optimal separation of gallic acids, J. Biosci. Bioeng. (2021).
[64] P.J. Xie, L.X. Huang, C.H. Zhang, F. You, Y.L. Zhang, Reduced pressure extraction of oleuropein from olive leaves (Olea europaea L.) with ultrasound assistance, Food Bioprod. Process. 93 (2015) 29–38.
[65] G. Ahmet, B. Cavit, F. Mehmet, Yılmaz,, Sesame bran as an unexploited by-product: Effect of enzyme and ultrasound-assisted extraction on the recovery of protein and antioxidant compounds, Food Chem. (2019).
[66] N. Elsayed, K.S.M. Hammad, E.A.E.S.A. El-Salam, Plum (Prunus domestica L.) leaves extract as a natural antioxidant: Extraction process optimization and sunflower oil oxidative stability evaluation, J. Food Process. Preserv. 44 (2020).
[67] W. Wu, S. Jiang, M. Liu, et al., Simultaneous process optimization of ultrasound-assisted extraction of polyphenols and ellagic acid from pomegranate (Punica granatum L.) flowers and its biological activities[J], Ultrason. Sonochem. (2021) 80.
[68] S. Chowdhury, S. Ghosh, K. Rashid, P.C. Sil, Deciphering the the role of ferulic acid against streptozotocin-induced cellular stress in the cardiac tissue of diabetic rats, Food Chem. Toxicol. 97 (2016) 187–198.
[69] M. Srinivasan, A.R. Sudheer, V.P. Menon, Ferulic acid: Therapeutic potential through its antioxidant property, J. Clin. Biochem. Nutr. 40 (2007) 92–100.
[70] V. Georgiev, A. Ananga, I. Dincheva, I. Badjakov, V. Gochev, V. Tsolova, Chemical Composition, In Vitro Antioxidant Potential, and Antimicrobial Activities of Essential Oils and Hydrosols from Native American Muscadine Grapes, Molecules 24 (2019).
[71] X. Yu, H. Zhang, J. Wang, J. Wang, Z. Wang, J. Li, Phytochemical Compositions and Antioxidant Activities of Essential Oils Extracted from the Flowers of Paeonia delavayi Using Supercritical Carbon Dioxide Fluid, Molecules 27 (2022).
[72] G.R. Pandey, M. Marimuthu, P. Kanagavalli, V. Ravichandiran, M. Veerapandian, Chitosanylated MoO3-Ruthenium(II) Nanocomposite as Biocompatible Probe for Bioimaging and Herbaceutical Detection, ACS Biomater Sci. Eng. 5 (2019).
[73] R.G. Prasad, Y.H. Choi, G.-Y. Kim, Shikonin Isolated from Lithospermum erythrorhizon Downregulates Proinflammatory Mediators in Lipopolysaccharide-Stimulated BV2 Microglial Cells by Suppressing Crosstalk between Reactive Oxygen Species and NF-kappa B, Biomol. Ther. (Seoul) 23 (2015) 110–118.
[74] H.W. Ryu, S.U. Lee, S. Lee, H.-H. Song, T.H. Son, Y.-U. Kim, H.J. Yuk, H. Ro, C.-K. Lee, S.-T. Hong, S.-R. Oh, 3-Methoxy-catalposide inhibits inflammatory effects in lipopolysaccharide-stimulated RAW264.7 macrophages, Cytokine 91 (2017) 57–64.
[75] C. Xia, Q. Meng, L.-Z. Lin, Y. Rojanasakul, X.-R. Wang, B.-H. Jiang, Reactive oxygen species regulate angiogenesis and tumor growth through vascular endothelial growth factor, Cancer Res. 67 (2007) 10823–10830.
[76] M. Lechner, P. Lirk, J. Rieder, Inducible nitric oxide synthase (iNOS) in tumor biology: The two sides of the same coin, Semin. Cancer Biol. 15 (2005) 277–289.
[77] S.I. Jang, Y.J. Kim, W.Y. Lee, K.C. Kwak, K.Y. Chai, Scoparone from Artemisia capillaris inhibits the release of inflammatory mediators in RAW 264.7 cells upon stimulation cells by interferon-gamma Plus LPS, Arch. Pharm. Res. 28 (2005) 203.
[78] S.G. Harris, J. Padilla, L. Koumas, D. Ray, R.P. Phipps, Prostaglandins as modulators of immunity, Trends Immunol. 23 (2002) 144–150.
[79] N. Zhang, J. Yeo, Y. Lim, P. Guan, Y. Cheng, Tuning the structure of monomeric amyloid beta peptide by the curvature of carbon nanotubes, Carbon 153 (2019) 717–724.
[80] S.-R. Kang, D.-Y. Han, K.-I. Park, H.-S. Park, Y.-B. Cho, H.-J. Lee, W.-S. Lee, C. H. Ryu, Y.L. Ha, D.H. Lee, J.A. Kim, G.-S. Kim, Suppressive Effect on Lipopolysaccharide-Induced Proinflammatory Mediators by Citrus aurantium L. in Macrophage RAW264.7 Cells via NF-kappa B Signal Pathway, Evid, Based Complement. Alternat. Med. (2011 (2011).).
[81] J. Li, W. Qian, Y. Xu, G. Chen, G. Wang, S. Nie, B. Shen, Z. Zhao, C. Liu, K. Chen, Activation of RAW 264.7 cells by a polysaccharide isolated from Antarctic bacterium Pseudoaltermonas sp S-5, Carbohydr. Polym. 130 (2015) 97–103.
[82] J.-A. Lin, C.-H. Kuo, B.-Y. Chen, Y. Li, Y.-C. Liu, J.-H. Chen, C.-J. Shieh, A novel enzyme-assisted ultrasonic approach for highly efficient extraction of resveratrol from Polygonum cuspidatum, Ultrason. Sonochem. 32 (2016) 258–264.
[83] A. Gorguc, C. Bircan, F.M. Yilmaz, Sesame bran as an unexploited by-product: Effect of enzyme and ultrasound-assisted extraction on the recovery of protein and antioxidant compounds, Food Chem. 283 (2019) 637–645.